SORPTION-MEDIATED CHEMICAL PROCESSES FOR THE VERSATILE TREATMENT OF PER- AND POLYFLUOROALKYL SUBSTANCES (PFAS) IN COMPLEX MEDIA

by

NAOMI GEVAERD DE SOUZA

Presented to the Faculty of the Graduate School of Civil Engineering

The University of Texas at Arlington in Partial Fulfillment

of the Requirements

for the Degree of

DOCTOR OF PHILOSOPHY

THE UNIVERSITY OF TEXAS AT ARLINGTON

August 2020

Copyright © by Naomi Gevaerd de Souza 2020

All Rights Reserved

Acknowledgements

First and foremost, I would like to acknowledge the guidance, support and expertise offered by my advisor, Dr. Hyeok Choi. Despite the countless failures inherent to research, Dr. Choi's confidence and determination anchored my efforts to persevere and we could finally accomplish many goals that seemed unattainable in the beginning.

Additionally, I wish to acknowledge the members of my committee Dr. Melanie Sattler, Dr. Srinivas Prabakar, and Dr. Junha Jeon for their genuine interest and valuable contributions throughout my graduate studies; Dr. Gautam Eapi for his impact on my career path; and Dr. Liangqiao Bien (Ben) for his guidance at the Shimadzu Institute. I must also credit my fellow teammates Dr. Wasiu Lawal, Akshay Parenky and Nusrat Chowdhury for the success obtained during my studies, and thank previous students that helped set up the lab and transmit the knowledge required to conduct research and assist in classes.

This research would not have been possible without the financial support of the Department of Civil Engineering through the Civil and Environmental Eng. STEM Doctoral Fellowship and the Civil Eng. John L. Mancini Scholarship, the University of Texas at Arlington through the Interdisciplinary Research Program and the Office of Graduate Studies through the Dissertation Fellowship Program, the Federal Student Aid through the Mav Doctoral and the Texas Public Education Grants, the Water Research Foundation through the Unsolicited Research Program (4877 (U2R16)), and the Environmental Research and Development Program under the Department of Defense (ER18-1482).

Finally, I would not be here today without the support and inspiration of all those whom I love so dearly. My eternal gratitude, respect, and profound love for my family; the true foundation of my life, and all my dearest friends that brough sunshine to my life.

July 30th, 2020

Abstract

SORPTION-MEDIATED CHEMICAL PROCESSES FOR THE VERSATILE TREATMENT OF PER- AND POLYFLUOROALKYL SUBSTANCES (PFAS) IN COMPLEX MEDIA

Naomi Gevaerd de Souza, PhD

The University of Texas at Arlington, 2020

Supervising Professor: Hyeok Choi

In recent years, per- and polyfluoroalkyl substances (PFAS) have gained notoriety due to environmental and health concerns. These molecules are chemically stable which contributes to their persistence in biological systems and their increased detections in surface waters. Treatment of highly persistent PFAS has been a challenging but significant task. The most practical technique for removal of PFAS is through adsorption onto granular activated carbon (GAC) or other novel materials. Meanwhile, PFAS are resistant to simple oxidation, and although decomposition of specific PFAS has been reported through advanced oxidation technologies, often energy-intense technologies capable of generating electrons such as ultraviolet radiation, microwave, or high temperatures are required when coupled with an oxidant to generate highly reactive radical species. The use of such technologies increases the cost and lowers its practical applicability. Hence, in an effort to develop a practical treatment technology, an adsorption-based decomposition technology was envisioned. The high surface area of GAC poses a unique opportunity of housing

reactive materials inside the pores. To achieve this, zero valent iron (ZVI), previously demonstrated to reductively delahogenate other persistent pollutants, was incorporated into the pores of the GAC, so called reactive activated carbon (RAC). Additionally, to generate highly oxidizing radical species persulfate (PS) was injected. Hence, once PFAS are encapsulated inside the pores, a combination of both reductive and oxidative species is present in close proximity to decompose the much recalcitrant PFAS. To demonstrate its effectiveness and understand its behavior, 6 PFAS of different functional groups and carbon chain lengths were investigated. An adsorption isotherm was first developed to test the affinity of the selected GAC. Then, the effects of reaction temperature, injection of PS, and presence of soil on removal of PFAS in water by RAC were evaluated. Results showed that RAC conjugated with PS at 60 ℃ exhibited decomposition of PFAS, exclusively all 3 carboxylic PFAS tested, obviously producing various identifiable short chain PFAS. Carboxylic PFAS were removed via physical adsorption combined with chemical decomposition while sulfonic PFAS were removed via solely adsorption mechanism. The presence of soil particles did not greatly affect the overall removal of PFAS. Carbon mass balance suggested that chemical oxidation by radical mechanisms mutually influences, in a complex manner, PFAS adsorption to GAC, ZVI and its iron derivatives, and soil particles. Nonetheless, all tested 6 PFAS were removed significantly. If successfully developed, the adsorption-mediated decomposition strategy may work for treatment of complex media containing PFAS and co-contaminants under different environmental settings. Future studies are required, to ensure the decomposition of PFAS exclusively inside the pores of RAC, additionally the synthesis of RAC containing different types of reactive metals and oxidants should be investigated. Pilot scale studies should also be conducted to simulate treatment beds and evaluate the effectiveness of the system.

Table of Contents

List of Figures

List of Tables

Chapter 1

Introduction

1.1 PFAS: resilient chemicals and ubiquitous pollutants

Per- and polyfluoroalkyl substances (PFAS) are a large class of synthetic organic chemicals with unique amphiphilic properties that are widely used in various industrial and commercial products(Wang et al., 2017). Since the 1950s, PFAS have been increasingly synthesized and utilized as surfactant agents and for treating surfaces of textiles, food packaging materials and metal surfaces such as nonstick cookware, industrial lubricant, additive in paints, pesticides, pharmaceuticals, and as a component in firefighting aqueous film-forming foams(Tanner et al., 2018; Sedlak et al., 2017; Lee et al., 2012; Hori et al., 2006).

PFAS encompass molecules of various molecular weights, and their basic structure is composed of a chemical functional group attached to a main alkyl chain which may be perfluorinated (carbons bonded to fluorides, C-F bonds) or polyfluorinated (carbons bonded to hydrogens and fluorides, C-F and C-H bonds) which imparts unique physicochemical properties to each compound and affects their affinity and reactivity(Buck et al., 2011). Due to the presence of the extraordinarily stable carbon-fluoride bonds with a high dissociation energy of 533 kJ/mol (Cagnetta et al., 2016). PFAS present great chemical stability (Xiao, 2017; Paul, Jones, and Sweetman, 2009).

When released from manufacturing plants or consumer products in the environment, several of the main PFAS precursors can be partially degraded into completely oxidized and more stable PFAS molecules such as perfluorooctane sulfonic acid (PFOS) and perfluorooctanoic acid (PFOA) through atmospheric oxidation, microbial

degradation or liver biotransformation (Tanner et al., 2018). However, further decomposition through hydrolysis, thermal degradation, photolytic or microbial degradation is difficult under natural conditions causing these chemicals to persist as recalcitrant pollutants (Tang et al., 2012).

Increasing concentrations of these compounds have been detected in various matrices such as water, sewage sludge, soil and sediment (Milinovic et al., 2015), with PFOS being the most abundant PFAS in natural waters around the world (Houde et al., 2011; Paul, Jones, and Sweetman, 2009). By 2002, phasing out of perfluorooctane sulfonyl fluoride substances (including PFOS) and perfluorooctace sulfonamide (PFOSA) production was carried out due to health and environmental concerns, however, smaller chain PFAS were used as substitutes in several products (Sedlak et al., 2017). As far as human exposure, likely sources are food (including leaching from PFAS-coated packaging), inhalation (indoor air in buildings with new carpeting), or point source exposure (occupational, or drinking water in certain locations) (Tanner et al., 2018).

Bioaccumulation has been observed for PFAS, in particular PFOS and PFOA; which can be detected in animal and human blood serum across the globe in both developed and developing countries (Tanner et al., 2018; Sedlak et al., 2017) with an overall higher concentration of PFOS (Kannan et al., 2004). Longer chains of PFAS such as PFOS and PFOA tend to bioaccumulate more than shorter chains, but the toxicity and mobility of shorter chains is still unclear (Sedlak et al., 2017). The toxicity of PFOS and PFOA has already been shown to be significant, mainly due to disruption of the endocrine, and immune systems, as well as indication of carcinogenicity for humans (Corsini et al., 2012; Milinovic et al., 2015; Rahman, Peldszus, and Anderson, 2014; Butenhoff et al., 2012).

Due to health and environmental concerns, the production of PFOA and PFOS by 3M, the major global manufacturer, was phased out in 2000 to 2002 (Buck et al., 2011)). In 2009, at the Stockholm Convention on Persistent Organic Pollutant, PFOS and its salts were added to the list of persistent organic pollutants (UNEP,2014). By 2012, the United States Environmental Protection Agency (USEPA) had listed six prevalent PFAS in the Third Unregulated Contaminant Monitoring Rule (UCMR3): PFOS, PFOA, perfluorononanoic acid (PFNA), perfluorohexanesulfonic acid (PFHxS), perfluoroheptanoic acid (PFHpA), and perfluorobutanesulfonic acid (PFBS) for monitoring and evaluation (USEPA, 2012). These six PFAS, in particular PFOA and PFOS, are commonly found in surface waters and soils and are persistent due to their highly oxidized states, presenting a challenge for environmental remediation (Li, Oliver, and Kookana, 2018; Park et al., 2009). In 2016, the USEPA published advisory levels in drinking water to 70 parts per trillion (ppt) for PFOA and PFOS (USEPA, 2016); and by 2018 the USEPA designated PFAS with long and short alkyl chain as national priorities to increase the know-how on precursor transformation products, exposure, fate and transport, and toxicity of PFAS including carboxylic acids, sulfonic acids and ethers (USEPA, 2018).

Currently, maximum contaminant levels are being discussed at national and state levels, with certain localities already approving more stringent regulations than then advisory levels proposed by EPA (Ateia et al., 2019). There is an increasing need for efficient remediation technologies for the treatment of PFAS-contaminated media.

1.2 Current Remediation Technologies for PFAS Treatment and Their Challenges

Conventional processes implemented in water treatment facilities are proven to be less effective against PFAS contamination (Rahman, Peldszus, and Anderson, 2014; Rayne and Forest, 2009). In a recent study evaluating water treatment efficiency in US plants, all six UCMR3 PFAS were detected in at least 90% of the source as well as treated waters at comparable concentrations, demonstrating that the traditional treatment strategies such as coagulation/flocculation, UV, ozonation, or activated carbon beds employed to control taste and odor are not effective in removing PFAS (Boone et al., 2019).

The most promising treatment methods may include activated carbon adsorption, along with membrane separation and ion exchange resins (Flores et al., 2013; Thompson et al., 2011). Adsorption process using granular activated carbon (GAC) made of lignite and bituminous coal, coconut shell, and biochar has been applied to remove PFAS in water (Appleman et al., 2013; Xiao et al., 2017; Carter and Farrell, 2010; Park et al., 2020).

In spite of its effectiveness, the process only physically separates PFAS, while not decomposing them at all, causing a secondary issue associated with regeneration of spent GAC and treatment of concentrated stream (Kucharzyk et al., 2017). Furthermore, even though long chain PFAS can be significantly removed, the removal of shorter chain and PFAS precursors is not effective or not yet elucidated (Ross et al., 2018).

Decomposition of PFAS is challenging due to the chemical inertness of these molecules, which is attributed to the strong, stable bond between carbon and fluoride (Trojanowicz et al., 2018). Because the carbon atoms in the hydrophobic tale are already in their most oxidized state, conventional oxidation is not an efficient strategy for treatment

of contaminated waters (Rahman, Peldszus, and Anderson, 2014; Rayne and Forest, 2009).

Meanwhile, successful reductive decomposition of halogenated chemicals (e.g., trichloroethylene and polychlorinated biphenyls) by using nanoscale materials such as metal particles in zerovalent states (i.e., zerovalent iron (ZVI; Fe^0)) has been often reported (Liu et al., 2005; Choi and Al-Abed, 2010). Zerovalent metals, while oxidizing in water, donate electrons (e^-), resulting in reductive dehalogenation of organic chemicals. Reduction processes, particularly those using zero valent iron (ZVI), have been successful in degrading different contaminants, including in situ remediation (Xie et al., 2014), The dehalogenation process, when occurring, is significant because PFAS, once defluorinated, become more vulnerable to chemical attack in subsequent oxidation processes. However, reductive defluorination of PFAS by ZVI, particularly highly-oxidized PFAS such as PFOS, has been reported only under specific lab conditions such as subcritical conditions(Hori et al., 2006) or in bimetallic systems under anoxic conditions (Zenobio et al., 2020).

Decomposition of PFAS through advanced oxidation processes (AOTs) has also been proposed, where highly reactive species such as hydroxyl radicals (HRs, $OH^{\bullet}$) and sulfate radicals (SRs, $SO_4^{\bullet-}$) readily attack organic chemicals (Anipsitakis and Dionysiou, 2004). However, decomposition of PFAS, in particular, perfluorinated alkyls, by the radical mechanism alone has been rarely reported. Consequently, AOTs commonly introduce other decomposition mechanisms through energy-intensive methods employing ultraviolet, microwave, ultrasound, electron beam, mechanical abrasion, gamma radiation and elevated temperatures(Merino et al., 2016; Vecitis et al., 2009; Lee et al., 2009; Wang et al., 2016). These energy intensive technologies are often a source of free electrons capable to reductively attacking PFAS molecules and simultaneously activating the PS.

The use of such energy sources reduces the practical applicability of the system for large scale applications and lead to higher cost of remediation.

Despite the variety of treatment technologies being currently studied, there is no comprehensive method available, particularly when considering removal and decomposition of a broad range of PFAS in large scale scenarios. Furthermore, there is no applicable, efficient mineralization method for these compounds that is not energy intensive other than removal as a treatment strategy.

1.3 Sorption-based Advanced Oxidation Proposal for PFAS treatment

Even though treatment for PFAS contaminated waters is challenging, the most promising and practical water treatment strategies incorporate adsorption for the removal of PFAS (Thompson et al., 2011; Flores et al., 2013; Appleman et al., 2014). Activated carbon, an effective and widely employed sorbent for water treatment, can be utilized as a granular or powdered material, but when employed in granular form (GAC), the pore size is large enough to house other reactive chemicals that may aid in degrading the target pollutants.

Transition metal in their elemental state are highly reactive and possess strong reducing capability due to their abundance of electrons making them good candidates for incorporation into GAC pores. One such transition metal is zero valent iron (ZVI), which has shown dehalogenation capabilities (Fu, Dionysiou, and Liu, 2014). ZVI is also capable of reacting with water to produce HRs and dihydrogen (Gu et al., 2017).Hori et al. (2006) demonstrated the capability of zero valent metals to reductively dehalogenate PFOS under sub-critical conditions and identified that amongst the tested metals, zero valent iron was the capable of decomposing PFOS to highest extent.

As previously determined, ZVI being an excellent free electron source and highly reducing agent can be impregnated into the adsorbent, working particularly well in the case of a mesoporous GAC with a high surface, large pore size and pore volume process that can harbor the nanoscale ZVI to produce a reactive activated carbon (RAC). The advantages of doing so involve, producing electrons capable of directly attacking the PFAS molecules. The encapsulation of these highly reducing and oxidizing species in the pores of the RAC would ensure its interaction with PFAS when present in proximity and possibly allow for defluorination. In previous studies it has been demonstrated that ZVI when impregnated into the pores of GAC successfully dehalogenated polychlorinated biphenyls (Choi, Al-Abed, and Agarwal, 2009).

Furthermore, in an effort to impart an oxidizing environment and employ AOTs, the addition of oxidants to the RAC can enhance the removal and defluorination of PFAS due to the generation of secondary radical species. HRs and SRs can be practically generated through activation of oxidants transition metals such as iron (Fe), so-called the Fenton-like reaction (Anipsitakis and Dionysiou, 2004).

Amongst some of the commonly used oxidants such as hydrogen peroxide, peroxymonosulfate, persulfate (PS; $S_2O_8^{2-}$), and potassium permanganate, only PS has shown to be highly reactive and capable of decomposing PFAS (Parenky et al., 2020). PS presents a high redox potential at E^0 = 2.01 V and is known to effectively produce SRs which are a better choice than HRs for direct electron transfer reaction for PFAS decomposition (Kolthoff and Miller, 1951; Bruton and Sedlak, 2017; 2018; Park et al., 2016; Liang and Su, 2009; Kim et al., 2018; Lee, Kim, and Park, 2018) Considering the highly oxidized nature of PFAS molecules, the higher efficiency of SRs is not surprising since it can abstract an electron from the oxygen group and destabilize the molecule while HRs mainly work through hydrogen abstraction (Li et al., 2017).

The RAC combined with oxidant system can expose PFAS to highly reducing and oxidizing radicals in a confined environment (RAC pores), thereby ensuring a highly reactive heterogenous system. Homogeneous reactions are also expected to occur in the liquid phase due to the solubility of iron species. Furthermore, shorter chain PFAS generated as reaction byproducts will also be subjected to RAC sorption and transformation reactions.

Considering the advantages and limitations of adsorption on GAC, reductive dehalogenation on ZVI, and advanced oxidation via radical mechanism, this research evaluates a complementary strategy to integrate the three PFAS removal processes.

The strategy involves using GAC impregnated with ZVI (RAC) in the presence of PS. PFAS can be concentrated onto GAC, where ZVI provides electrons for reductive decomposition and provides Fe ions to activate PS for the production of radicals.

Since PFAS are highly packed in a confined space, i.e., RAC surface, uniquely ensuring closer exposure to in-situ generated reactive species, the processes, in a cooperative manner, may synergistically remove and decompose PFAS in water.

In this this study, 6 different PFAS of high environmental interest (all of those listed in the UCMR3) with varying carbon chain length and functional group are evaluated to give a comprehensive understanding of the behavior of various PFAS and help in understand the effect of parameters such as functional group and alkyl chain length on the adsorption and decomposition process.

Furthermore, the impact of soil particles on the reaction is also examined due to the environmental relevance of treating mixed media contaminated with PFAS. A mass balance is also attempted to understand the partitioning of parent and byproduct PFAS within the system.

1.4 Study Objectives

The overall goal of this study is to combine physical adsorption, reductive defluorination, and advanced oxidation into a versatile and practical system capable of removing and decomposing PFAS of environmental concern.

The main objectives of this study are:

1) To determine the PFAS sorption capability of the GAC base and its partitioning behavior.

2) To integrate decomposition with adsorption in the synergistic system of RAC and oxidant and examine the capacity of the system to remove and decompose selected PFAS.

3) To examine the performance of the reactive system when in complex media (presence of soil particles) to understand partitioning and treatment efficiency.

Chapter 2

Literature Review

2.1 PFAS Classification

PFAS have been defined as

> "*aliphatic substances containing one or more C atoms on which all the H substituents present in the nonfluorinated analogues from which they are notionally derived have been replaced by F atoms, in such a manner that PFASs contain the perfluoroalkyl moiety* C_nF_{2n+1}— "

with the distinction that perfluoroalkyl substances contain all H substituted by F while polyfluoroalkyl substances contain at least one C where all H have been replaced by a F in a way to present the perfluoroalkyl moiety (Buck et al., 2011). "PFCs", a common term has been to describe several fluorinated compounds, has been designed to describe perfluorocarbons exclusively, which comprises of chemicals that contain only F and C atoms (OECD, 2015).

These broad definition of PFAS encompass several thousand synthetic substances, including polymeric and non-polymeric compounds such as polytetrafluoroethylene and PFOA, respectively. Figure 2.1 extracted from OECD (2013) shows a diagram of the current PFAS classification.

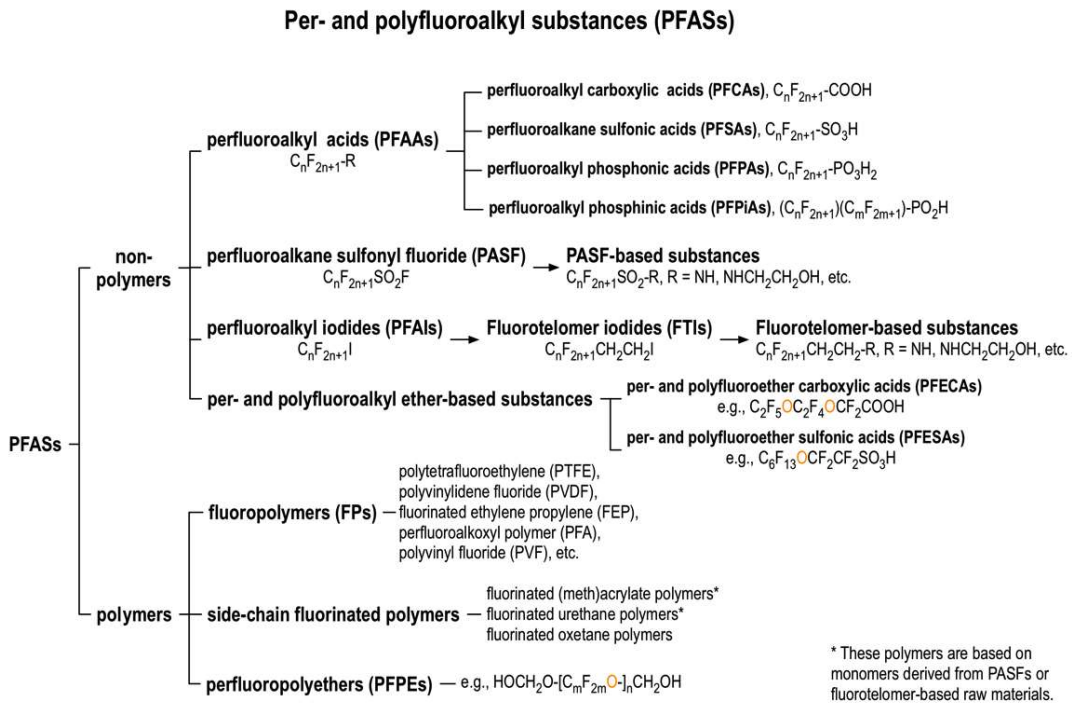

Figure 2-1: General classification of PFAS (extracted from OECD (2013)).

Amongst the non-polymeric compounds, the most notorious PFAS are perfluoroalkyl acids carboxylic and sulfonic acids, namely PFOA and PFOS. Their general structure is represented in Fig 2.2 below.

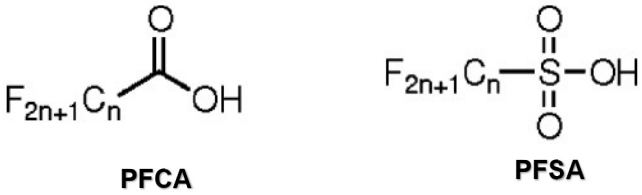

Figure 2-2: General structure of PFCA and PFSA extracted from Rayne and Forest (2009).

The chain length of a PFAS is another important characteristic relevant to PFAS classification. Depending on the functional group, different definitions apply to determine what is considered a “long-chain PFAS”; in the case of perfluoroalkyl carboxylic acids (PFCA) they must present 7 or more perfluorinated carbons (8 C or more in total), and for perfluoroalkane sulfonates (or perfluoroalkyl sulfonic acids, PFSA) long chains present 6 or more perfluorinated carbons (7 C or more in total) (OECD, 2013)

Amongst the UCMR3 PFAS, long-chain PFCA include PFNA and PFOA, while for PFSA the compounds PFOS and PFHxS are listed. The other two compounds listed, PFHpA and PFBS are short-chain PFAS under this definition. The molecular structure of these six UCMR3 PFAS consists mainly of a hydrophobic tail, composed of fluorinated carbons, and a hydrophilic head, comprised of a specific functional group as shown of Fig 2-3 below.

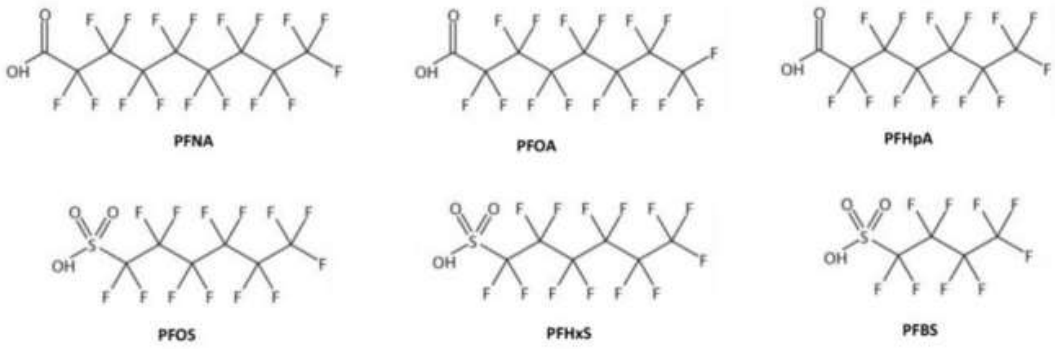

Figure 2-3: Molecular structure of the six PFAS listed in the UCMR3.

After the phasing out of long-chain PFAS such as PFOA and PFOS, short-chain PFAS were explored more abundantly as viable substitutes in many commercial applications even though they present a lower performance and may require higher amounts of perfluorinated compounds ((Lindstrom, Strynar, and Libelo, 2011). PFAS with shorter chains present a higher hydrophobicity, which affects their solubility, fate and

mobility, detection, and toxicity which are not still clearly understood; the lack of data is also evident in the prevalence of studies published on long-chain PFAS (Ateia et al., 2019).

2.2 Sorption Processes and PFAS Behavior

Sorption processes encompass several subcategories of molecule interaction such as absorption, in which sorbate molecules are incorporated into a sorbent, and adsorption, in which the sorbate adhere to the surface of a sorbent. Adsorption can be classified as chemisorption, when there is a chemical bond between sorbate and sorbent that is more permanent in character with bond forces of 60-450 kJ/mol; and physisorption, that involves van der Waals forces, dipole forces, dipole-dipole forces, and induction forces bellow 50 kJ/mol (Kammerer, Carle, and Kammerer, 2011; LeVan, Carta, and You, 1999). Sorption processes can occur as a single layer, or a multilayer of sorbate molecules. Desorption, or regeneration of the sorbent, is achievable in physisorption; also, physisorption is usually a faster process than chemisorption (Kammerer, Carle, and Kammerer, 2011; LeVan, Carta, and You, 1999). In practice it is very difficult to differentiate these processes because commonly they occur simultaneously and are affected by several external parameters such as temperature and pH as well as the intrinsic physical-chemical properties of the materials such as the potential for an ionic charge. The kinetics of sorption reactions are also affected by mass transport of the sorbate to the surface of the sorbent, number of available sites at the sorbent and/or multi-layer interactions (Kammerer, Carle, and Kammerer, 2011).

In regard to PFAS, sorption processes determine innumerous aspects of their impact to humans and the environment. Fate and transport, and toxicity is affected by how

PFAS get absorbed into cells, or their accumulation on adsorbents such as soil particles or minerals, and their partitioning into natural waters.

When considering fate and transport of PFAS in the environment, the comparison between different characteristics of the soils including pH, dissolved organic carbon, cation exchange capacity and particle size distribution revealed that the main sorption process was due to a hydrophobic interaction between the fluorinated tail and the organic matter in the soil (Milinovic et al., 2015). In certain aspects, it seems that the soil mineral fraction composition is not as important as the presence of organic matter, and the overall hydrophobicity of the PFAS plays an important in sorption, with longer chains being more hydrophobic and attaching more to soils with high organic content (Milinovic et al., 2015; Zhao et al., 2014). Soil/sediment organic matter (SOM) is a complex matrix of difficult characterization, but humic substances are the major constituents of SOM (Zhao et al., 2014). When comparing sorption of PFOS onto different humic substances, the major attraction force seemed to be polar forces as opposed to hydrophibicity as reported for soils in general (Zhao et al., 2014). The high affinity of PFAS for organic matter was also noted when evaluating wastewater sludge, where higher concentrations of organics could be related to higher PFAS concentrations (Wang et al., 2015).

PFAS have also been observed to adhere to mineral substrates, including positively and negatively charged materials such as zeolites, silica-based materials, and metals such as iron and iron oxides. The effect of cations and anions in soil is also important, but there is not clear indication of which type of soil or mineral content will present higher sorption capacities from the available dataset, perhaps due to inconsistent characterization of such materials across various researches (Li, Oliver, and Kookana, 2018; Ochoa-Herrera and Sierra-Alvarez, 2008).

Other complicating factors in predicting sorption behavior onto soils is that different length PFAS also seem to present different sorption characteristics, and the presence of other pollutants such as hydrophobic hydrocarbons also affects sorption of perfluorinated compounds (Li, Oliver, and Kookana, 2018). When comparing two analogous C8 PFAS, PFOA and PFOS sorption to soils, for example, it was noted that PFOS sorption is highly irreversible when compared to PFOA. That difference may be attributed to the fact that PFOS has more C-F units that PFOA, making it more hydrophobic (Milinovic et al., 2015).

Some of the mechanisms conceptualized as relevant in PFAS sorption processes onto soils include hydrophobic interaction with organic matter, ligand binding through divalent cations, electrostatic interaction with positive charges on mineral and organic phases, and electrostatic interactions with oxides (Li, Oliver, and Kookana, 2018). The sorption of PFAS onto environmental matrices such as soil is not clearly elucidated, but it is clear that this phenomenon plays an important role in determining fate and transport of these chemicals in nature. It must be considered that PFAS' sorption onto solid materials also affects their concentration in the water column not only due to partitioning onto the liquid phase, but due to the presence of suspended solids and organic matter in solution.

PFAS present unique sorption characteristics. These amphiphilic molecules can potentially be sorbed into either hydrophilic or hydrophobic sorbates. Many PFAS present moieties that are ionic or ionizable, such as carboxylic acids and hydroxyl groups and fall under IOCs (ionic and ionizable organic compounds) (Kah et al., 2017). These compounds present a positive or a negative charge over a wide pH range, unlike neutral compounds (Kah et al., 2017). For the most environmentally relevant PFAS, PFOA and PFOS, the acid dissociation constant is extremely low ($pKa<1$) and these compounds are mostly deprotonated in natural conditions. For PFAS acids with low pKa, the molecules will be present in anionic form and are likely to sorb to positively charged sorbents through

electrostatic forces; but other parameters such as ionic strength will also affect sorption due to compression of the electrical double layer (Merino et al., 2016).

Commonly, in the case of neutral sorbates, the more hydrophobic the sorbent, the greater the attraction and sorption of the target chemical; in this case, the partitioning could be represented by a single coefficient (K_{ow}, water/octanol partitioning coefficient) (Kah et al., 2017).However, for IOCs a single coefficient is not sufficient to explain the partitioning behavior of these molecules; these molecules, as well as neutral compounds, are also affected by the mechanism of size exclusion in the case of porous solid sorbents because pore size can cause mass transport limitations for the sorbate. Besides pore size, the nature of the sorbent plays an important role in sorption of IOCs; the composition at the surface of the sorbent, particularly in carbonaceous materials such as biochar, may present heteroatoms and functional groups that can strongly attract ionic compounds (Kah et al., 2017).

Removal of PFAS was also observed in negatively charged sorbents such as negatively charged silica, perhaps due to hydrophobic interactions of the fluorinated tail and the hydrophobic sorbent surface (Merino et al., 2016). In general, it has been observed that longer fluorinated chains increase the hydrophobicity of the PFAS (Milinovic et al., 2015), and longer chains were better adsorbed onto activated carbon substrate (Merino et al., 2016; Milinovic et al., 2015).

Removal efficiency seems to improve with the presence of air bubbles due to the higher concentration at the water/air surface layer, partitioning of the fluorinated tail into air and the polar head remaining in solution (Merino et al., 2016). Sorption of PFAS onto certain synthetic polymer resins and ion exchangers was reported to be more efficient than natural material sorbents such as activated carbon (Merino et al., 2016). The resins may

be regenerated with methanol, but longer chain PFAS require larger amounts of the solvent to remove these chemicals (Merino et al., 2016).

PFAS can be removed from solution through sorption onto carbonaceous sorbents. Two main interactions, electrostatic and hydrophobic, seem to be the sorption main mechanisms for PFAS (Merino et al., 2016). A particularly important carbonaceous sorbent is activated carbon; it is produced by the pyrolysis of hard woods, coconut shells, coal, bones etc. and a subsequent chemical or physical activation that will increase its porosity with surface areas in the range of 500 to 3000 square meter per gram of substrate (m^2/g) (Kammerer, Carle, and Kammerer, 2011; Kah et al., 2017).

Functional groups in the surface may allow the formation of hydrogen bonds, which may increase sorption or reduce by repulsion charge of ionic sorbents; hydrogen bonds are particularly important in fluorinated compounds as they are formed between electronegative atoms (fluorine, nitrogen and oxygen) and the electropositive hydrogen nucleus of functional groups such as hydroxyl (Kah et al., 2017). Understanding sorption of these molecules onto different materials can help develop a removal strategy for treating municipal waters and diminishing public exposure to these harmful chemicals.

2.3 Treatment Strategies for PFAS

2.3.1 Non-destructive strategies

Over the past decade there has been significant progress in developing treatment technologies capable of removing PFAS. Amongst some of the legacy removal techniques such as GAC and ion exchange, research has been conducted on other removal techniques such as nano-filtration, reverse osmosis and electrocoagulation (Merino et al. ,2016). Additionally, removal of PFAS has also been achieved using mineral based

adsorbent materials such as alumina, montmorillonite and hematite as listed in Table 2-1. The removal efficiency through each of techniques varies widely on the type of material used and PFAS tested. Novel adsorbents materials with a framework are also being evaluated such as cross-linked cyclodextrin, cross-linked alkoxysilicanes, porous aromatic frameworks and show promising results (Ross et al., 2018) Many studies have been conducted only on a single solute solution and often evaluating only PFOA and PFOS as seen in Table 2-1.

Although these newly developed materials are capable of removing PFAS to a large extent, studies have typically only been conducted on a laboratory scale and are yet to be demonstrated for real-world large-scale application due to their varying efficacy when considering PFAS of different chain length (Ross et al., 2018). Furthermore, once these materials have been used for PFAS removal, its regeneration capacity and safe disposal have not been elucidated. Amongst the previously mentioned adsorbents, the most widely applied technologies are GAC and ion exchange due to their relatively low cost and capability of regeneration (Appleman et al., 2013). Although these removal techniques are capable of removing PFAS from the contaminated media, the regeneration of GAC often requires harmful chemicals and extreme conditions to achieve high regeneration efficiency while disposal of GAC may lead to contamination based on the method of disposal (Gagliano et al., 2020).

Table 2-1: Adsorption technologies employed for PFAS removal in water treatment.

Technology	PFAS treated	Citation
Nano-filtration	PFOA, PFOS, PFBS, PFHxS, PFNA, PFPeA, PFHxA, PFDA	Appleman et al., 2013
Reverse osmosis	PFOS	Tang et al., 2007)
Alumina	PFOA, PFOS	Wang and Shih, 2011
Montmorillonite, kaolinite, hematite	PFOS, PFHxS, PFOA, PFHxA	Zhao et al., 2014
GAC	Several PFAS	Appleman et al., 2013
Amberlite (ion exchange)	PFOS	Xiao et al., 2012
Cyclodextrin	PFOA	Xiao et al., 2017

2.3.2 Destructive strategies

The decomposition of PFAS is highly challenging due to the presence of multiple C-F bonds, which are some of the strongest bonds in organic chemistry. There is also the concern that degradation of PFAS chemicals processes generates shorter chain PFAS that can be more mobile or toxic that their precursors (Ross et al., 2018).

Degradation techniques can be divided into two main categories, one involving non-radical mechanism and the other involving radical mechanism. Non-radical mechanism of decomposition involves techniques such as high temperature thermal decomposition by addition of amendment, incineration at nearly 1000 ℃ and microbial degradation. The nucleophilic behavior of hydroxide ions and calcium oxide lead to the degradation of PFAS at temperatures ranging from 350-600 ℃ whereas without the addition of amendments, much higher temperatures of 1000 ℃ are required (Wu et al. 2019; Wang, Lu, et al., 2015). A study conducted by Aleksandrov et al. (2019) investigated the potential of conversion of polytetrafluoroethylene (PTFE) into PFAS and found that

negligible amount of PFAS was being formed through incineration. Another study conducted by (Solo-Gabriele et al., 2020) found that low amounts of PFAS were detected in municipal waste ash suggesting that PFAS was not completely degraded during incineration leading to some amount of undecomposed PFAS, but the contribution from the ash was far less compared to that from construction waste in landfill leachate.

Few studies have reported microbial degradation of PFAS, while biodegradation has been observed for polyfluorinated alkyls and other precursors, degradation of highly oxidized perfluoroalkyls such as PFOA and PFOS has been rarely observed apart from a study reporting *Acidimicrobium* sp. being capable of removing and partially defluorinated PFOA and PFOS (Huang and Jaffé, 2019; Liu et al., 2010)

Radical based decomposition techniques are more widely applied for PFAS decomposition. A key component of radical based technology is the addition of oxidants which are capable of producing radicals. Upon supplying energy to these oxidants, the cleavage in the bonds produce highly reactive radical species which can directly attack the PFAS molecules. The most common ways of supplying this energy is through heat, UV, sonolysis or transition metals (Merino et al., 2016).

The generation of radicals such as HRs and SRs through these methods are capable of directly attacking PFAS molecules and decomposing PFAS (Wang and Wang, 2018). In addition to SRs and HRs recent studies have demonstrated the decomposition of PFAS by the addition of sulfite or iodide in combination with UV capable of generating electrons to reductively defluorinated PFAS (Gu et al., 2017). In order to improve decomposition of short-chain PFAS in these systems, addition of cationic polymer has also been applied to promote the formation micelles which has shown to improve decomposition of PFOS(Chen et al. 2020).

Sonolysis is a technology where in the energy produced through sound at high frequencies causes cavitation, drastically increasing pressure and temperature inside the collapsing bubbles aiding in PFAS decomposition (Campbell and Hoffmann, 2015).

Electro-chemical decomposition of PFAS has been well demonstrated using specially modified electrodes that can surpass the activation energy needed to degrade PFAS such as boron-doped diamond electrode and titanium oxide (Ti_4O_7) (Ochiai et al., 2011; Lu Wang et al., 2020).

Transition metal such as cobalt when used in combination with peroxymonosulfate was capable of decomposing a polyfluoroalkyl substance (6:2 fluorotelomer sulfonate) but not for PFOA or PFOS (Zhang et al., 2020). In decomposing PFAS, PS has been more widely used in comparison to PMS and HP. A catalyst such as Fe-modified diatomite with persulfate was capable of decomposing PFOA (da Silva-Rackov et al., 2016). Another similar metal based catalyst, Mg-aminoclay. when combined with persulfate was capable of decomposing PFOA (Arvaniti et al., 2015). As previously seen, metal-based activators/catalyst when combined with oxidants can potentially decompose PFAS under ambient conditions.

Chapter 3

Materials and Methods

3.1 Chemicals and Reagents

PFNA (heptadecafluorononanoic acid, $C_9F_{17}O_2H$, CAS 375-95-1), PFOA (pentadecafluoro-1-octanoic acid, $C_8F_{15}O_2H$, CAS 335-67-1), PFOS (heptadecafluorooctanesulfonic acid potassium salt , $C_8F_{17}SO_3K$, CAS 2795-39-3), and PFBS (potassium nonafluoro-1-butane sulfonate, $C_4F_9SO_3K$, CAS 2940-49-3) were obtained from Sigma-Aldrich (St. Louis, MO). PFHpA (tridecafluoroheptanoic acid, $C_7F_{13}O_2H$, CAS 375-85-9) and PFHxS (tridecafluorohexane-1-sulfonic acid potassium salt, $C_6F_{13}SO_3K$, CAS 3871-99-6) were purchased from Synquest Laboratories (Alachua, FL) and Frontier Scientific (Logan, UT), respectively. Isotopically marked standards for parent and byproduct PFAS (composition displayed in Table A-1 in the Appendix) were obtained as mixtures in methanol from Wellington Laboratories (Guelph, ON, Canada).

Iron nitrate nonahydrate ($Fe(NO_3)_3 \cdot 9H_2O$), sodium borohydride ($NaBH_4$), sodium hydroxide (NaOH), and sodium persulfate ($Na_2S_2O_8$) were obtained from Sigma-Aldrich. Acetonitrile (ACN, C_2H_3N), methanol (CH_4O), formic acid (CH_2O_2), fluoride standards and ionic strength adjuster (ISA, Hach, Loveland, CO) were acquired from Thermo Fisher Scientific (Waltham, MA).

Large molecule separation (LMS) solid phase extraction (SPE) cartridges (25 mg, 1 mL) shown in Fig. 3-1 were purchased from Agilent Technologies (Santa Clara, CA). Polyethersulfone (PES) syringe filters (0.22 μm pore size, 13mm) manufactured by Foxx Life Sciences (Salem, NH) were purchased through Thermo Fisher Scientific.

All stock solutions and reactions were prepared with ultrapure water (18 MΩ·cm) produced by a Millipore Milli-Q filtration system (Billerica, Massachusetts).

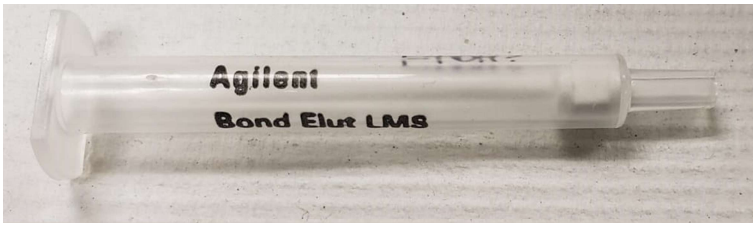

Figure 3-1: LMS cartridge utilized for sample cleanup. The cartridge is packed with a polymeric sorbent for separation of the target analytes.

The granular activated carbon utilized in this project, variety Hydrodarco® 3000 (HD 3000, CAS 7440-44-0), was kindly donated by Cabot Norit Americas (Marshall, TX). HD3000, described by the manufacturer as an acid washed carbon produced by high temperature steam activation of lignite coal indicated for water treatment, was exclusively used as a base GAC because it shows a well-developed mesoporous structure capable of harboring ZVI nanoparticles (Choi et al., 2008).

The soil utilized in this study was collected from a site within the university campus (Arlington, TX), sieved through #35 sieve, and dried overnight in an oven at 103 ℃ prior to use.

3.2 Synthesis and Characterization of Materials

3.2.1 Synthesis of RAC

Synthesis of RAC was conducted by in-situ incorporating ZVI particles into GAC, as developed by (Choi et al., 2008). In brief, 22.8 g of $Fe(NO_3)_3 \cdot 9H_2O$ was melted at 60 ℃ in 5 mL of ultrapure water and added into 10 g of GAC. After a 6-hour drying period, the slurry was calcinated in a furnace through a stepwise method where temperature was increased at 180 ℃/h, held for 1h at 150 ℃ and for 4h at 300 ℃. After cooling, unintegrated

Fe particles and small size GAC/Fe granules were removed by using a #20 sieve. The resulting RAC with incorporated iron (as Fe_2O_3) was then reduced to elemental iron by resuspending 4 g of RAC in 50 mL methanol/DI water (30/70, v/v), raising the pH above 6.5 through dropwise addition of 5 N NaOH solution, and slowly adding a 20 mL aqueous solution containing 1.6 g of dissolved $NaBH_4$. Then, 4 g of GAC/Fe was added into 50 mL of methanol/water (30/70 v/v) and pH was raised to 6.5 by using 5 N NaOH, to which 1.6 g of $NaBH_4$ dissolved in 20 mL of water was drop-wise added to reduce Fe in GAC to elemental Fe^0. The borohydride reduction was carried for 3 h until there was no more evident hydrogen gas evolving from the mixture. Finally, the RAC retained at the no. 20 sieve was rinsed thoroughly with methanol and dried overnight. Fresh RAC was prepared prior to each batch experiment.

3.2.2 Characterization of RAC

The structural properties of the RAC including Brunauer, Emmett, and Teller (BET) surface area were determined by using a Tristar 3000 (Micromeritics, Norcross, GA) porosimetry analyzer.

The surface morphology was investigated with a scanning electron microscope (SEM, Hitachi S-4800II FE-SEM, Tokyo, Japan) and Fourier transform infrared spectroscopy (FTIR; Thermo Fisher Scientific Nicolet 6700) was used to find any changes in chemical bonds.

3.2.3 Soil characterization

Organic content in soil was briefly determined through gravimetric analysis associated with the loss-on-ignition method as previously described by (Ghabbour et al., 2014).Briefly, a soil sample was weighted in an aluminum dish as shown in Fig. 3-2, dried

overnight at 103 ℃ and re-weighted, and fired up in a furnace at 500 ℃ for 5 h for complete volatilization of the organic content and weighted again after cooling in a desiccator. The soil was also evaluated with a porosimetry analyzer.

Figure 3-2: Aluminum dish loaded with soil and activated carbon for gravimetric characterization.

3.3 Batch Experiments

3.3.1 GAC sorption studies

Adsorption experiments were conducted simultaneously for 10 days at room temperature (20 ℃) in 20 mL, capped polypropylene (PP) sacrificial batch reactors containing 20 mL of 10 mg/L PFAS at unregulated pH conditions. Adsorption experiment was conducted in 20 mL of a capped polypropylene reactor containing 20 mL of 10 mg/L PFAS under unregulated pH conditions. All isotherms were obtained employing single-solute batch experiments. The GAC was employed for the adsorption experiments in concentrations of 0.25, 0.5, 0.1. 0.2, 0.3, 0.5. 0.75, and 1 g GAC/L. GAC was employed at varying concentrations of 0.025-1.0 g GAC/L. Prior to use, the activated carbon was thoroughly washed with deionized water and dried overnight at 70 ℃. Sample collection

occurred at predefined intervals, at 0.5, 2, 5, 8, 24, 48, 72, 120, 168 and 240 h. All adsorption kinetic and equilibrium data were obtained through sacrificial batch experiments, where one reactor under agitation at 120 rpm by a rotary shaker (shown in Fig. 3-3(a)) was sacrificially taken at each time interval up to 240 h for sample collection and analysis (spent reactors and collected samples shown in Fig. 3-3(b)).

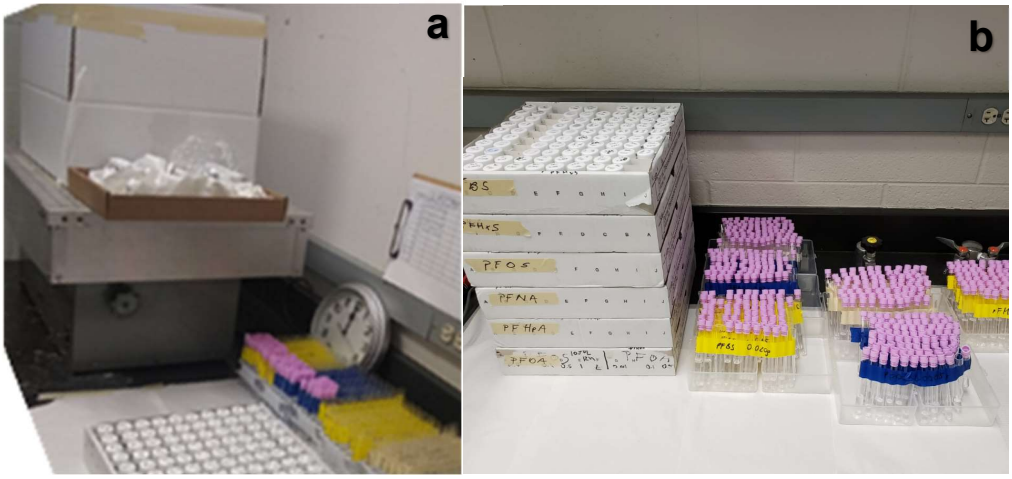

Figure 3-3: GAC adsorption studies setup showing the rotary shaker (a), the spent reactors and collected samples (b) .

3.3.2 RAC sorption and reactivity studies

RAC experiments were conducted in 20 mL, capped PP batch reactors. Heated experiments were conducted in a sand bath as seen in Fig. 3-4. Reactions were monitored for 24 h with samples collected at predetermined times. RAC was used at 20 g/L and PS was injected to achieve 0.3 M which is comparable to those used in previous studies (Wang and Wang, 2018). Reaction temperatures were controlled at 20-60 ℃ while pH was not

controlled to avoid any interferences caused by buffer species. Later 20 g/L of soil was also added into batch reactor to evaluate the impact in the treatment's performance.

Figure 3-4: Sand bath utilized to conduct heated reactions.

3.4 Sample Treatment and Chemical Analysis

3.4.1 Sample treatment

Sample aliquots of 200 µL of were drawn at predetermined intervals and diluted to 2 mL of ultrapure water in 8 mL PP tubes. Sample cleanup was conducted by passing 1 mL of the diluted sample through a 0.22 µm PES syringe filter for subsequent SPE procedure. SPE LMS cartridges were preconditioned with 1 L methanol, followed by 1 mL ultrapure water, and then loaded with 500 µL of the sample. After rinsing the cartridge with 1 mL of ultrapure water, the analytes were eluted with 1 mL M/S grade methanol and placed in PP autosampler vials for analysis through liquid chromatography tandem mass spectrometry (LC-MS/MS). Isotopically marked PFAS standard mixtures were added to the sample prior to extraction (extraction standard), and prior to analysis (injection standard).

3.4.2 Solid phase desorption

Desorption of PFAS from the solid phase was achieved by using a mixture of organic solvent (to desorb hydrophobic alkyl chains) and sodium salt (to desorb anionic head groups) as described elsewhere(Gagliano et al., 2020). After reaction time completion, the reactor was centrifuged at 3000 rpm for 15 min, the supernatant discarded, and 20 mL of methanol along with 30 µL of 0.1 N NaOH were added back into the container. After 60 min of sonication bath in a 8891 Cole Parmer Ultrasonic (Vernon Hills, IL, shown in Fig. 3-5) followed by 15 min of centrifugation, aliquots of 200 µL were drawn and diluted in methanol to 2 mL in 8 mL PP culture tubes. Samples were filtered through a 0.22 µm PES syringe filter and centrifuged for 15 min at 3000 rpm prior to collection into PP autosampler vials for analysis. The extraction procedure was repeated 3 times per reactor.

Figure 3-5: 8891 Cole Parmer sonicator used for desorption of target PFAS from solid phase present in reaction vials.

3.4.2 PFAS chemical analysis

PFAS were analysed using a Shimadzu Nexera X2 (Nakagyo-ku, Kyoto, Japan) liquid chromatographer (LC) coupled with a Shimadzu 8040 triple quadrupole mass spectrophotometer (MS). Mobile phase was 0.1% formic acid in water and ACN, with a flow rate set at 0.3 mL/min and a binary gradient where ACN contribution was increased from 30% to 90% over 6 min, held at 90% for 3 min, and ramped down back to 30% over 3 min. Separation was carried out using an Agilent Zorbax Eclipse C18 RRHD (50 mm x 3 mm x 1.8 µm particle size) column. Sample injection volume was 10 µL. Target analytes (parent and byproducts) were measured using multiple reaction monitoring according to the Table B-1 in Appendix B as previously described (Bruton and Sedlak 2017).

3.4.3 Fluoride chemical analysis

Concentration of free fluoride ions in solution was monitored with a Hach (Loveland, CO) HQ440d multi meter assembled with IntelliCAL™ Fluoride ISEF121 capable of detecting up to 0.01 mg/L F^-. Commercially available fluoride standards of 0.5, 1 and 2 mg-F^-/L were utilized for calibration and system check. For sample collection and analysis, 500 µL of sample and 500 µL of ISA solution were mixed into a 10 mL PP vial caps and values were read after stabilization.

Chapter 4

Results

4.1 GAC and RAC characterization

The commercially available activated carbon produced from lignite coal (GAC HD 3000) which was used as the base material for this research, and the synthesized RAC (Fe + GAC) were evaluated and characterized as explained previously. The results are described in this section.

4.1.1 Raw and synthesized materials

Figure 4-1 shows a macroscopic view of the carbonaceous sorbents utilized for the experiments. The grain size of the base GAC after sieving was observed in average to range from around 2 to 5 mm in diameter as displayed in Fig. 4-1(a). Once the $Fe(NO_3)_3$ was incorporated via the wet insipient wetness method and subsequent calcination, the appearance of the material drastically changed to an intense red shade indicating the presence of oxidized iron species as seen in Fig. 4-1(b). The Fe-incorporated GAC was then reduced through $NaHB_4$ and the final product, reduced RAC, presented a much darker tone as shown in Fib. 4-1(c) suggesting a successful reduction of the iron to zero valent state.

4.1.2 SEM characterization

The microscopic morphology of the base GAC was evaluated under SEM and revealed a porous surface as shown in Fig. 4-2. The freshly synthesized RAC visible in Fig 4-3, presented spherical particles present on the surface believed to be the incorporated iron. Figure 4-4 shows the spent RAC, i.e., RAC subjected to a 24-h chemical reaction at

60 ℃ with 10 mg/L PFAS and 0.3 M PS. The sharp structures observed are believed to the salt crystals from the oxidant and the PFAS.

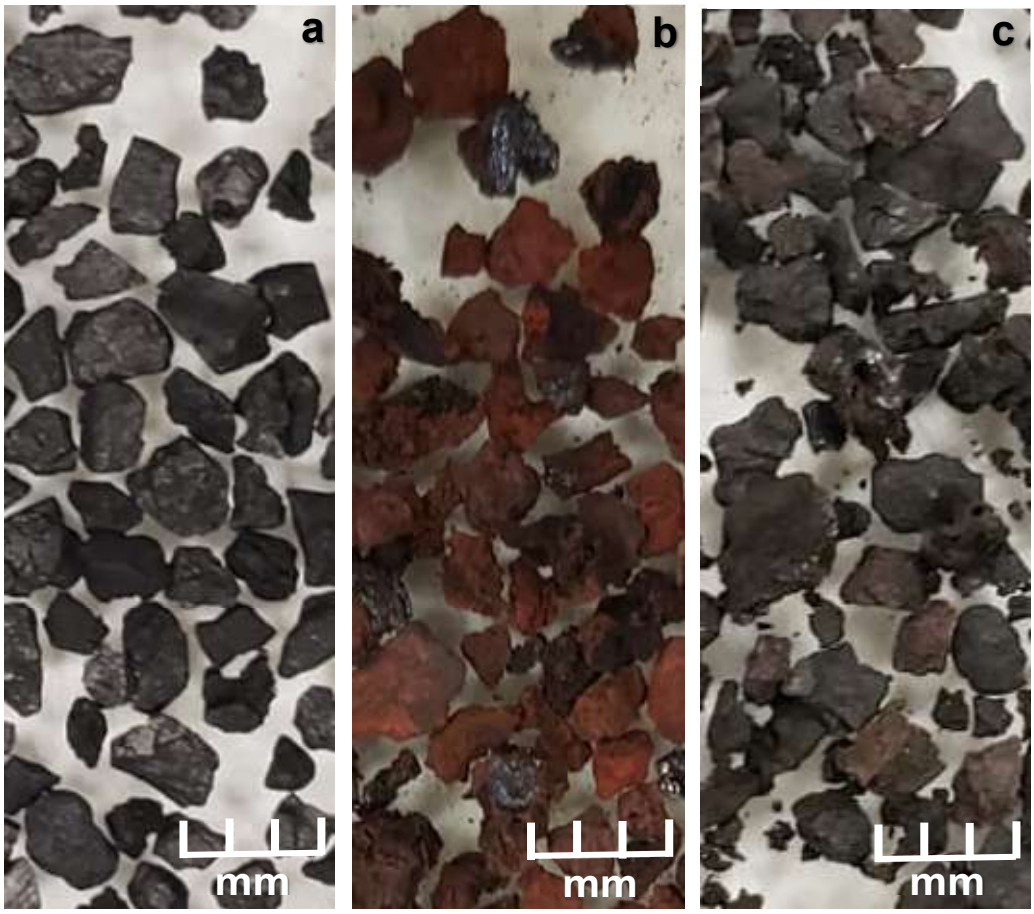

Figure 4-1: Detailed image of (a) commercially available GAC Hydrodarco® HD 3000, (b) GAC incorporated with $Fe(NO_3)_3$ or so-called unreduced RAC, and (c) GAC incorporated $Fe(NO_3)_3$ and reduced with $NaBH_4$ or so-called reduced RAC.

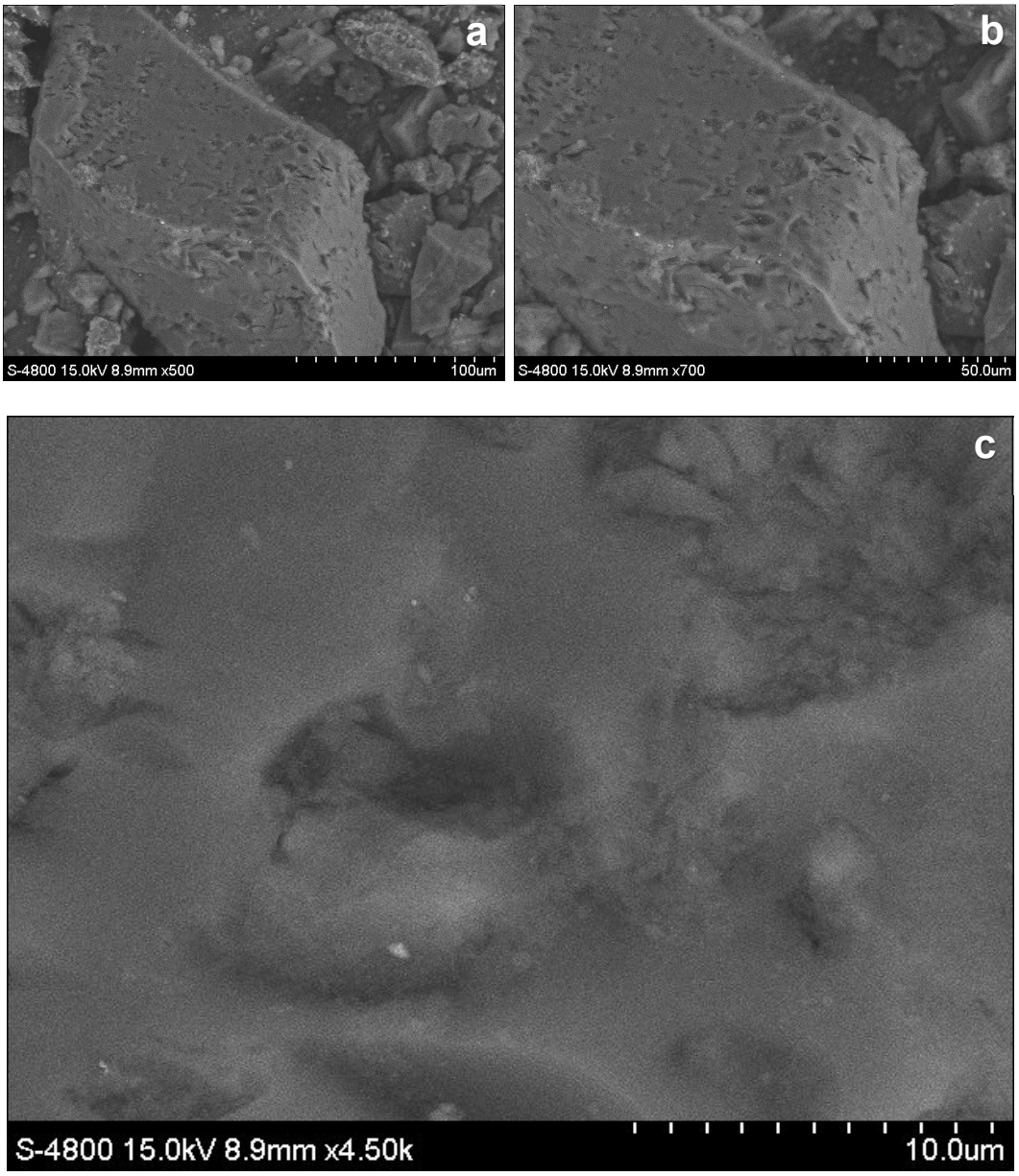

Figure 4-2: Microscopic details of the base material GAC HD 3000 obtained through SEM at (a) 500, (b) 700, and (c) 4,500 times magnification. The porous characteristic of the GAC is evident.

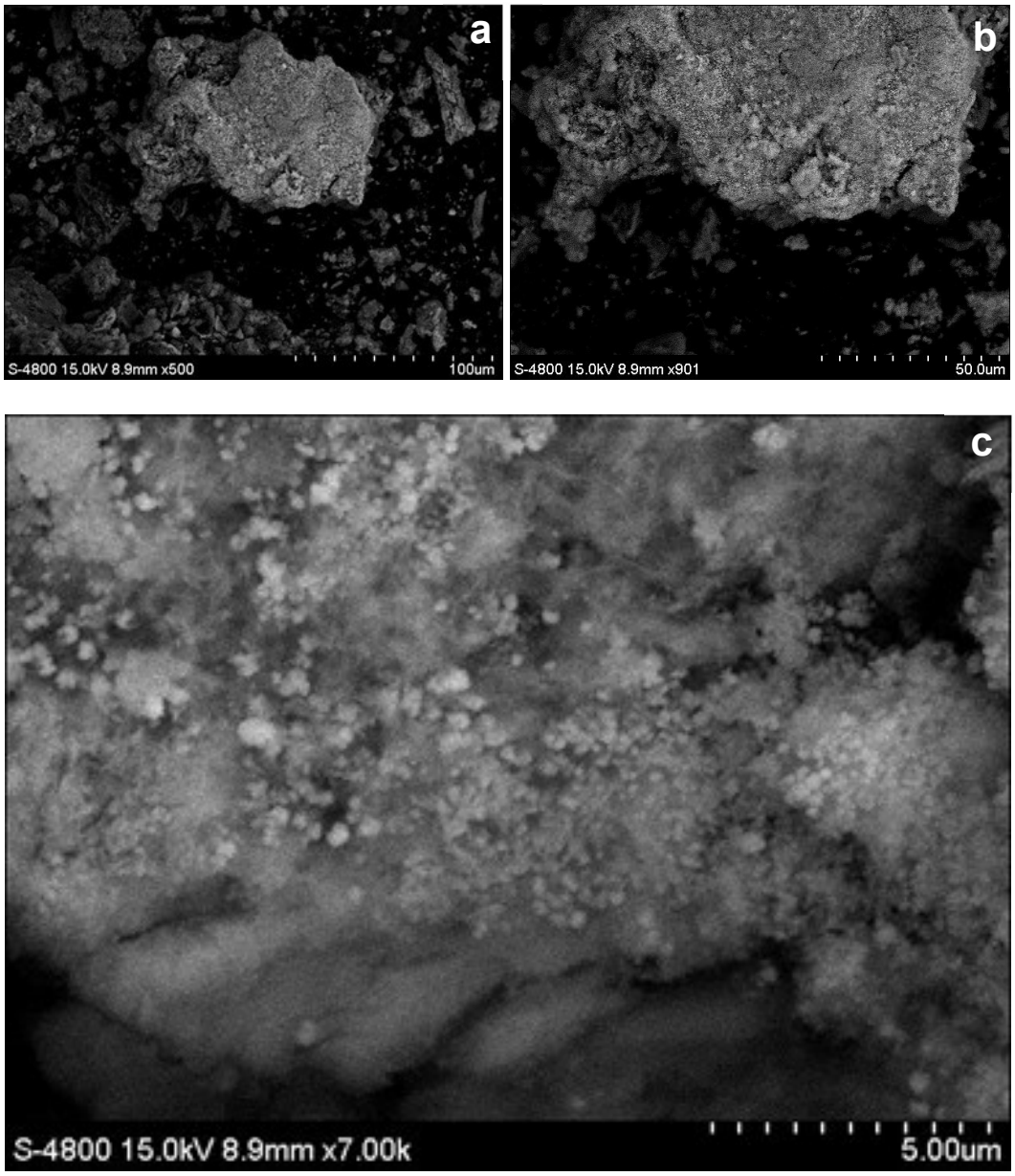

Figure 4-3: Microscopic details of the synthesized, reduced RAC obtained through SEM at (a) 500, (b) 900, and (c) 7,000 times magnification. The surface presents smaller spherical particles believed to be incorporated iron.

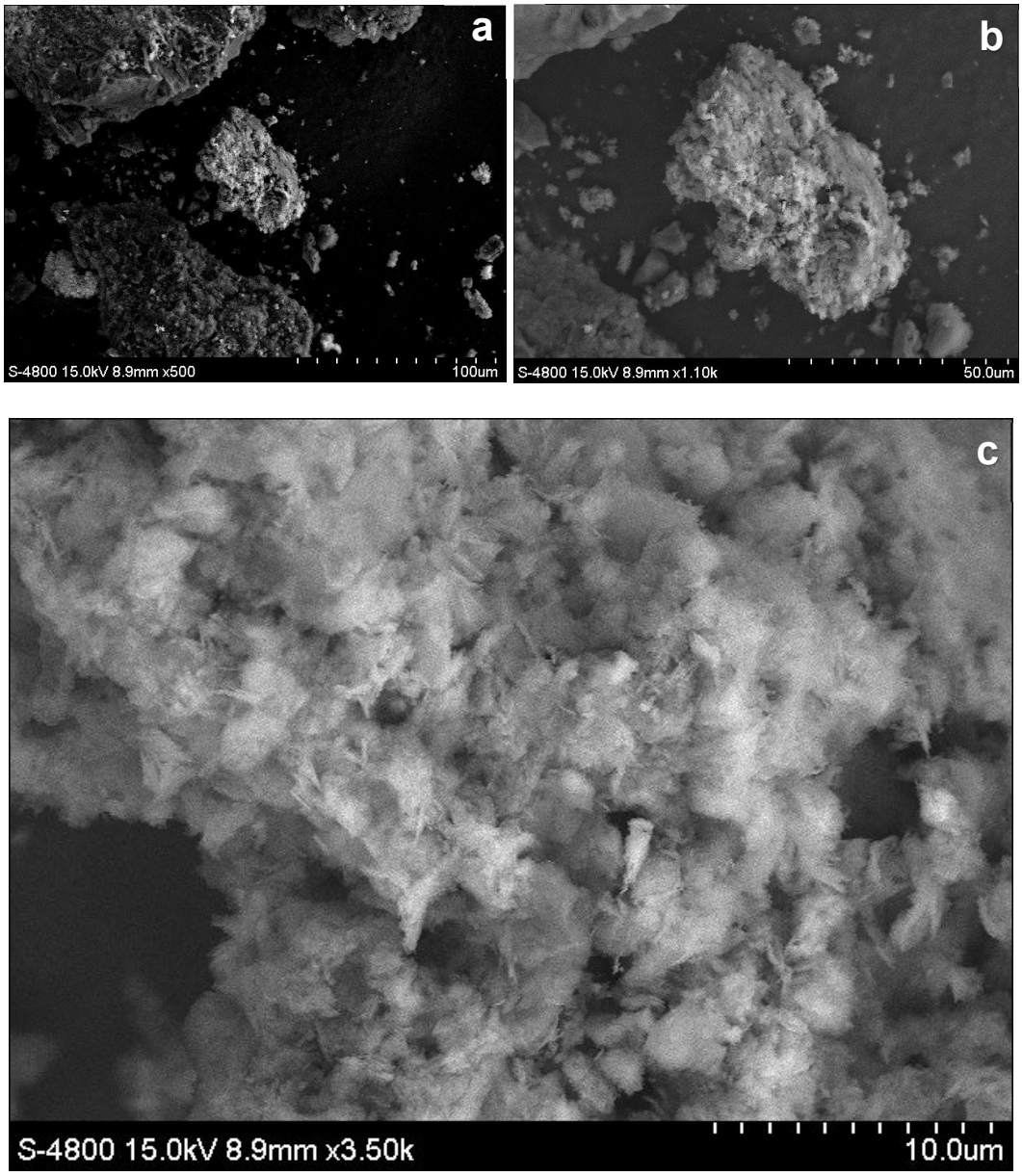

Figure 4-4: Microscopic details of the spent RAC (RAC exposed to PFOS, PS and temperature of 60℃ for 24 h) obtained through SEM at (a) 500, (b) 1,100, and (c) 3,500 times magnification. The sharp structures are believed to be crystal salts of PS and PFAS.

4.1.3 Porosimetry analysis

The characterization of the pore structure through porosimetry and nitrogen sorption evaluation of the carbonaceous materials and soil is summarized in Table 4-1. GAC and RAC nitrogen sorption and desorption isotherms are also listed in Appendixes C and D, respectively. The BET surface area of GAC was at 593 m^2/g, while the synthesized RAC presented 336 m^2/g and their mesoporous structure at 2-50 nm was confirmed, as well characterized elsewhere (Choi et al., 2008). Due to the successful incorporation of iron into the pores of the GAC, the fresh RAC had a reduction is adsorption sites demonstrated by a reduction of 43% in the surface area, and 48% reduction in pore volume.

To evaluate the physicochemical property changes associated with the treatment strategy, the structural properties of the synthesized RAC were also evaluated for two samples of spent RAC, namely RAC/PFAS (after exposure to 10 mg/L PFAS during 24 h at a temperature of 60 ℃), and RAC/PS/PFAS (after exposure to 10 mg/L PFAS and 0.3 M PS during 24 h at a temperature of 60 ℃). The surface area decreased from 336 m^2/g in the fresh RAC to 224 m^2/g (33%) in RAC/PFAS, and 93 m^2/g (73%) in RAC/PS/PFAS suggesting pore occupancy by the target sorbate along with the oxidant added to the reaction. The modification in sorptive capacity in the case of GAC exposed to heat-activated PS has been well documented, and has been attributed to the occupancy of the sorption sites by sulfate ions produced during the activation of PS as well and sodium and sulfur residuals, the effects of acidic and oxidative exposure of the GAC material and subsequent alterations of the surface chemistry (Hutson, Ko, and Huling, 2012).

The soil used in certain experiments was also evaluated and revealed a low surface area of 7 m^2/g, while pore measurements could not be determined.

Table 4-1: Structural properties of fresh GAC, fresh RAC, spent RAC after 24-h reaction with PFAS at 60 ℃, spent RAC after 24-h reaction with PFAS and PS at 60 ℃, and fresh soil.

Property	Fresh GAC	Fresh RAC	Spent RAC RAC/PFAS	Spent RAC RAC/PS/PFAS	Fresh soil
BET surface area (m^2/g)	**593.2**	**336.2**	**224.0**	**93.3**	**6.8**
BJH adsorption cumulative surface area [a] (m^2/g)	110.7	66.4	47.9	15.8	2.1
BJH desorption cumulative surface area[a] (m^2/g)	194.1	107.4	83.3	28.4	3.8
Total pore volume (cm^3/g)	**0.2074**	**0.1068**	**0.0724**	**x**	**x**
BJH adsorption cumulative pore volume [a] (cm^3/g)	0.2172	0.1196	0.0977	0.0377	0.0044
BJH desorption cumulative pore volume [a] (cm^3/g)	0.2619	0.1366	0.1133	0.0413	0.0056
BET average pore diameter (4V/A by BET) (nm)	**1.398**	**1.271**	**1.292**	**1.351**	**x**
BJH adsorption average pore diameter (nm)	7.844	7.207	8.167	9.572	8.483
BJH desorption average pore diameter (nm)	5.399	5.089	5.441	5.824	5.996

[a]of pores between 1.7 and 300 nm.

4.1.4 FTIR spectroscopy analysis

FTIR spectra for fresh GAC and RAC, as well as spent RAC/PFAS and RAC/PS/PFAS in the range of 4000 to 500 cm^{-1} in show in Fig 4-5. Clearly there are changes in chemical bonds as the GAC undergoes Fe incorporation and is exposed to the reaction environment. Due to the heterogeneous nature of the GAC composition, and the broad nature of the peaks, it is difficult to clearly identify which molecular bonds are being affected.

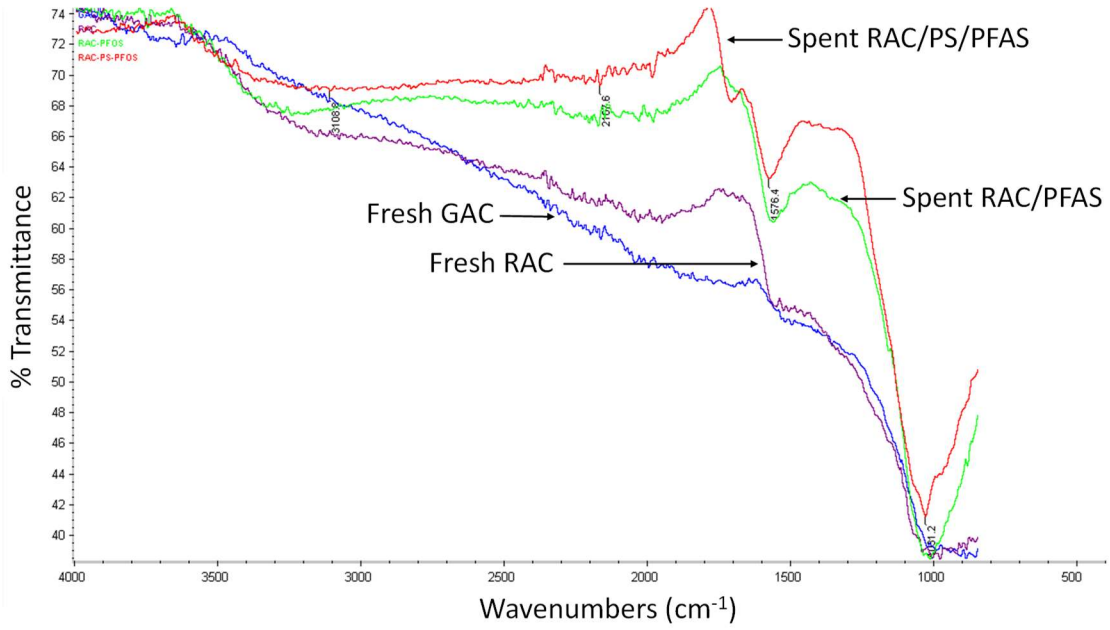

Figure 4-5: FTIR spectra of fresh GAC, fresh RAC, RAC interacting with PFOS, and RAC interacting with PFOS in the presence of PS.

4.1.5 Soil gravimetric analysis

Organic content in the soil tested in this study was briefly determined through gravimetric analysis associated with the loss-on-ignition method revealing a 0.011% organic carbon in weight.

4.2 Adsorption of PFAS in water on GAC

4.2.1 PFAS adsorption kinetics

It is important to evaluate the affinity of the specific mesoporous GAC selected in this study (i.e., HD3000 made of lignite coal) for the 6 target PFAS listed in the UCMR 3 because it is a base material for placement of ZVI particles and thus for fabrication of RAC to implement the overall treatment strategy, i.e., adsorption-mediated decomposition of PFAS.

Adsorption batch experiments were conducted at fixed PFAS concentration at 10 mg/L and varying GAC concentration at 0.025-1.0 g/L, resulting in PFAS:GAC ratio of 1:2.5-100. Adsorption kinetics of the three carboxylic PFAS in this study, PFNA, PFOA, and PFHpA, are shown in Fig 4-6, while Fig 4-7 demonstrates the adsorption kinetics of the three sulfonic PFAS studied: PFOS, PFHxS, and PFBS. As expected, higher amounts of GAC adsorbed more PFAS. In all cases, adsorption equilibria were achieved after around 72-120 h.

Adsorption kinetics of 6 PFAS at a fixed amount of GAC at 0.2 g/L were compared in Fig. 4-8, suggesting that all PFAS have very similar affinity for GAC under the tested conditions.

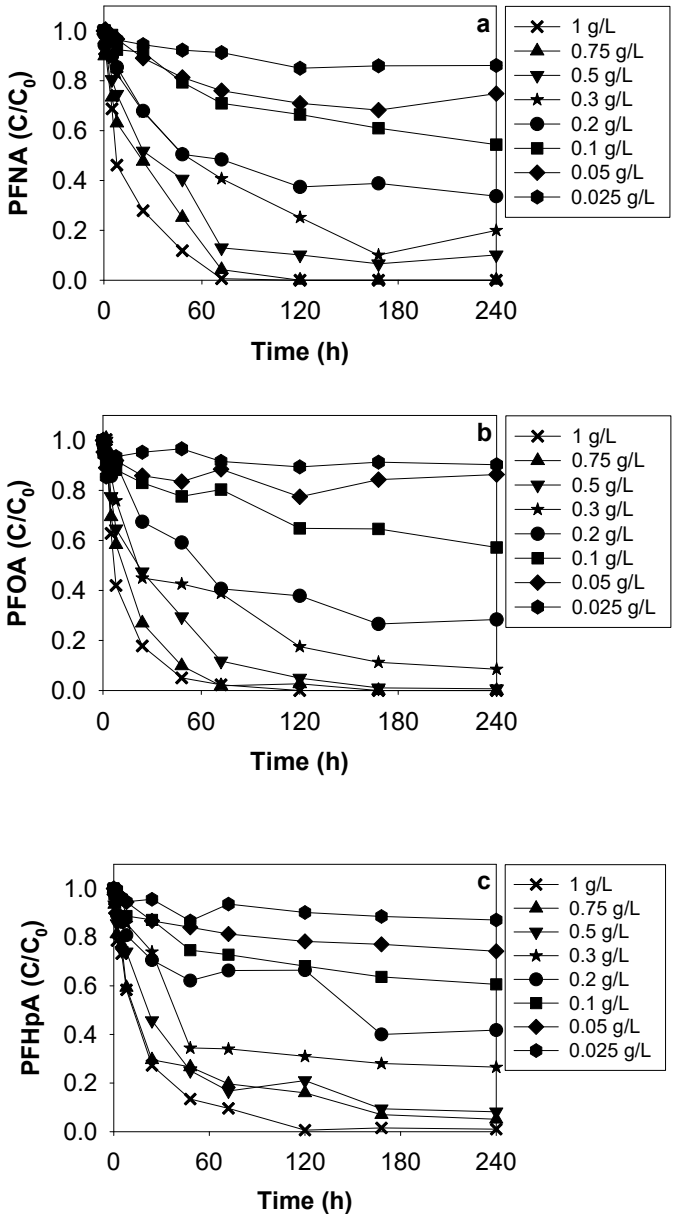

Figure 4-6: Removal of aqueous (a) PFNA, (b) PFOA, and (c) PFHpA by GAC at various loadings under ambient conditions (PFAS 10 mg/L; GAC 0.025 to 1 g/L; no soil; no PS; 20 ℃; 1 atm; and initial pH 4.5 to final pH around 6.0 (no pH control)).

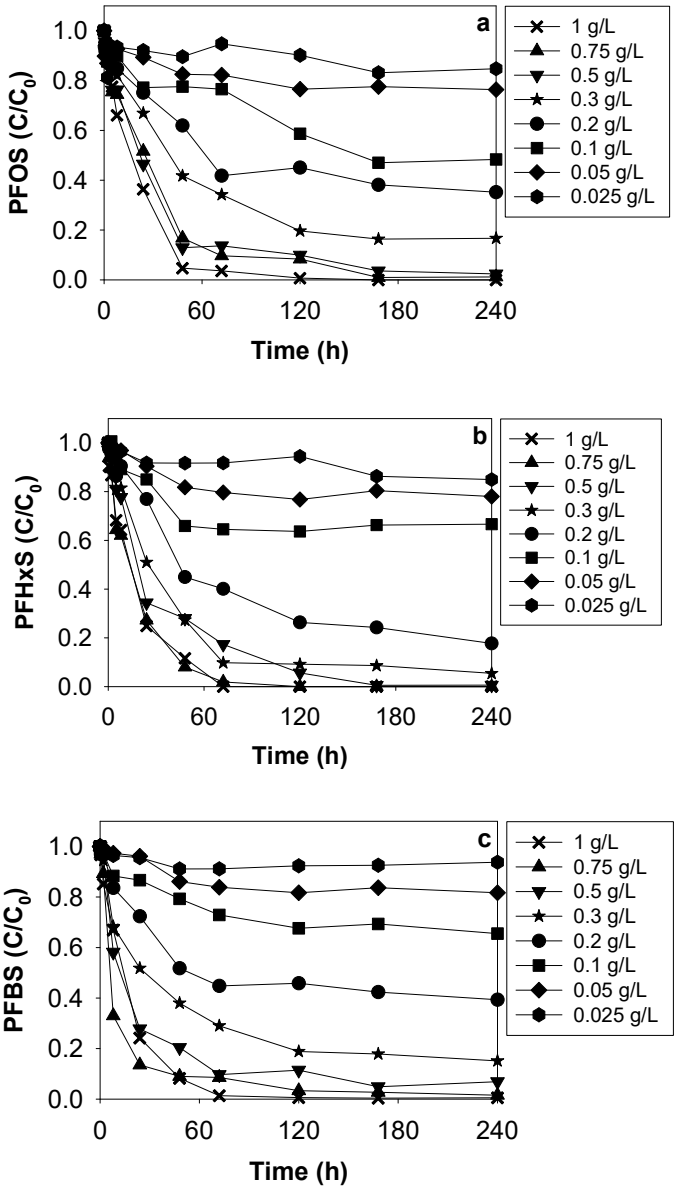

Figure 4-7: Removal of aqueous (a) PFOS, (b) PFHxS, and (c) PFBS by GAC at various loadings under ambient conditions (PFAS 10 mg/L; GAC 0.025 to 1 g/L; no soil; no PS; 20 ℃; 1 atm; and initial pH 4.5 to final pH around 6.0 (no pH control)).

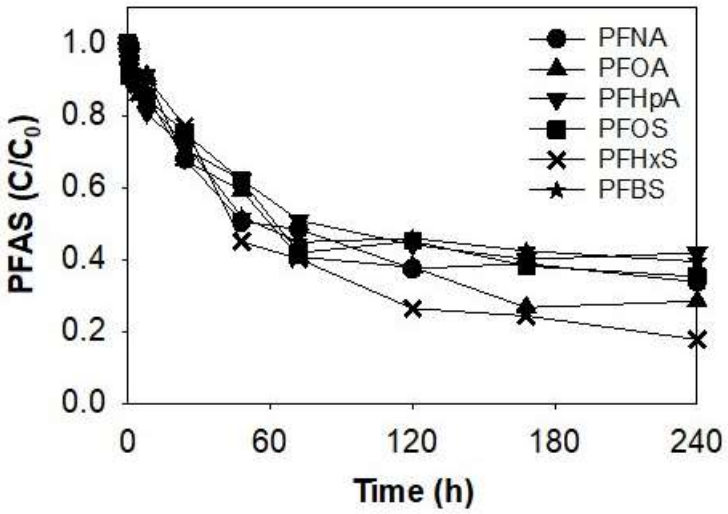

Figure 4-8: Removal of various aqueous PFAS by GAC under ambient conditions (PFAS 10 mg/L; GAC 0.2 g/L; no soil; no PS; 20 ℃; 1 atm; and initial pH 4.5 to final pH around 6.0 (no pH control)).

4.2.2 Adsorption isotherms

Adsorption isotherms of PFAS onto GAC were developed, as shown in Fig. 4-9 and the Langmuir and Freundlich models were applied to best fit the data, as summarized in Table 4-2. Two models were comparable. In the Langmuir model, maximum adsorption capacity was ranged from 30.12 mg-PFAS/g-GAC for PFBS to 77.52 mg-PFAS/g-GAC for PFNA. In the Freundlich model, all PFAS showed 1/n much less than 1, implying nonlinear adsorption. Based on the Langmuir model, longer chain PFAS, except for PFOA, were generally adsorbed more in order of PFNA>PFOS>PFHpA>PFHxS>PFBS, and PFOS, as 8-carbon PFAS (C8), was absorbed more than PFOA, as also reported elsewhere (Gagliano et al., 2020; Ochoa-Herrera and Sierra-Alvarez, 2008). Overall, HD3000 was effective to adsorb PFAS.

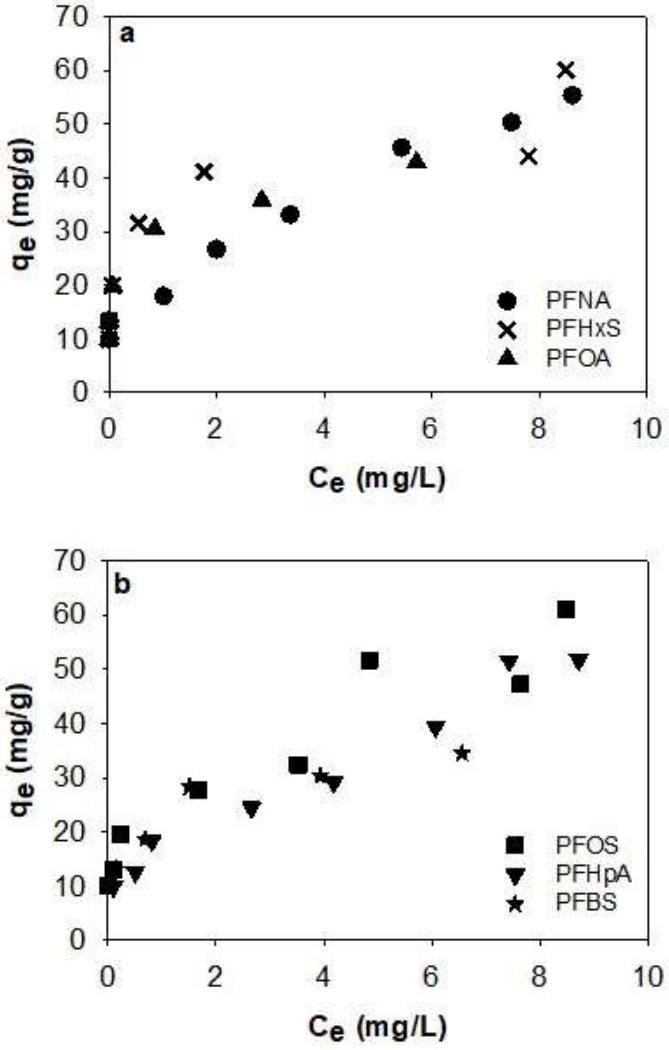

Figure 4-9: Adsorption isotherms of (a) PFNA, PFHxS and PFOA and (b) PFOS, PFHpA and PFBS in water onto GAC under ambient conditions (PFAS 10 mg/L; GAC 0.025 to 1 g/L; no soil; no PS; 20 ℃; 1 atm; and initial pH 4.5 to final pH around 6.0 (no pH control)).

Table 4-2: Langmuir and Freundlich isotherm parameters for adsorption of PFAS on to GAC.

PFAS	Langmuir Isotherm*			Freundlich Isotherm*		
	Q_m	K_L	r^2	K_F	1/n	r^2
PFNA	77.52	0.26	0.9811	18.11	0.520	0.9954
PFOA	33.11	7.02	0.9170	29.05	0.115	0.6142
PFHpA	58.48	0.05	0.8598	19.77	0.383	0.9354
PFOS	60.24	0.81	0.8997	26.79	0.315	0.9286
PFHxS	47.85	2.40	0.8704	33.20	0.164	0.7481
PFBS	30.12	14.43	0.9344	20.76	0.229	0.8849

* Langmuir isotherm constants Qm (mg PFAS/g GAC) and K_L (L/mg), and Freundlich isotherm constants K_F [(mg PFAS/g GAC)/(mg PFAS/L)$^{1/n}$] and 1/n (PFAS 10 mg/L; GAC 0.025 to 1 g/L; no soil; no PS; 20 ℃; 1 atm; and initial pH 4.5 to final pH around 6.0 (no pH control)).

4.3 Removal of PFAS in water by RAC

ZVI particles were impregnated into GAC. Its BET surface area was decreased from 593 m^2/g to 336 m^2/g and other characterization results using SEM and FTIR were comparable to those extensively described by Choi et al. (2008), implying successful incorporation of ZVI nanoparticles in size of 20-30 nm to the mesoporous structure of GAC.

4.3.1 Effect of temperature

Reactivity of RAC with 3 carboxylic PFAS and 3 sulfonic PFAS in water was evaluated in the absence of PS at 20-60 ℃ to check if PFAS are removed and decomposed, as shown in Fig 4-10. In all cases, significant amounts of PFAS were removed from the aqueous phase. Three general trends were found. First, higher temperature in order of 60 ℃>40 ℃>20 ℃ was more favourable for removal of PFAS. Second, longer chain PFAS were removed more in order of PFNA>PFOA>PFHpA within carboxylic PFAS and PFOS>PFHxS>PFBS within sulfonic PFAS. Third, PFOS (C8) was removed marginally more than PFOA (C8).

Since ZVI has shown great reactivity with halogenated chemicals via reductive dehalogenation and higher temperatures may accelerate the reaction kinetics, the observed removal of aqueous PFAS was expected to be ascribed to decomposition of PFAS on RAC [16]. However, targeted LC/MS analysis was not able to find any significant byproducts from either the liquid or solid phases, implying there was no significant decomposition of PFAS under the conditions and thus removal of PFAS was solely due to their adsorption to RAC.

.

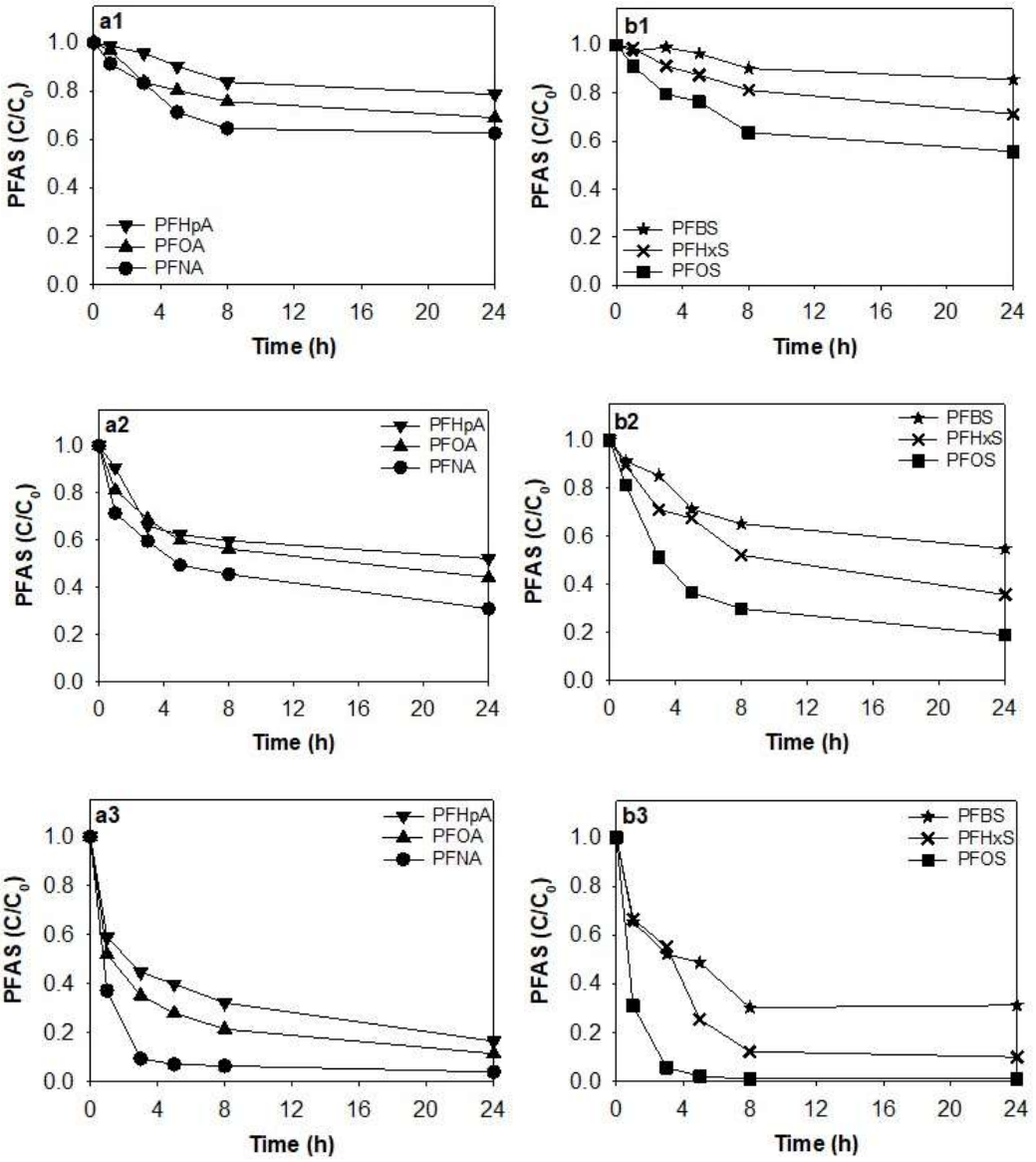

Figure 4-10: Removal of aqueous (a) carboxylic PFAS and (b) sulfonic PFAS in water by RAC at (1) 20 ℃, (2) 40 ℃, and (3) 60 ℃ (10 mg/L PFAS; 20 g/L RAC; no soil; no PS; 20-60 ℃; 1 atm; and initial pH around 9 to final pH around 8 (no pH control)).

This finding is also indirectly supported by the fact that the last two trends mentioned above are the same as the results from adsorption of PFAS onto GAC. Formation of Fe oxides and Fe hydroxides around core ZVI due to its oxidation has been reported [37]. Higher temperatures are expected to rapidly oxidize ZVI to various Fe derivatives which also remove PFAS via either adsorption or complexation mechanism (Parenky et al., 2020; Gagliano et al., 2020; Ochoa-Herrera and Sierra-Alvarez, 2008; Choi, Al-Abed, and Agarwal, 2009; S. Park, Zenobio, and Lee, 2018)

4.4 Removal of PFAS in water by RAC conjugated with oxidant

4.4.1 Effect of persulfate

The same experiments in Fig. 4-10 was revisited in the presence of an oxidant, PS at 0.3 M, as shown in Fig. 4-11. General PFAS removal trends were the same between the presence and absence of PS. Three findings were noticeable. First, removal efficiency of PFAS slightly decreased with the addition of PS, most probably due to loss of adsorptive sites in RAC by PS and its derivatives. Second, addition of PS in an unbuffered system quickly dropped pH from 9 to 2 in 1 h due to scavenging reactions of PS with water molecules to produce H^+, O_2, and SO_4^- (Zhang et al., 2019). PS can be activated by Fe ions released from ZVI and produces various reactive radical species such as SRs and HRs depending upon reaction pH and similar phenomenon was also observed for PS conjugated with unmodified activated carbon (Wang and Wang, 2018). In general, acidic condition is favourable for generation of SRs which are better species than HRs for direct electron transfer reaction to decompose PFAS and byproducts (Liang and Su, 2009; Wacławek et al., 2017).

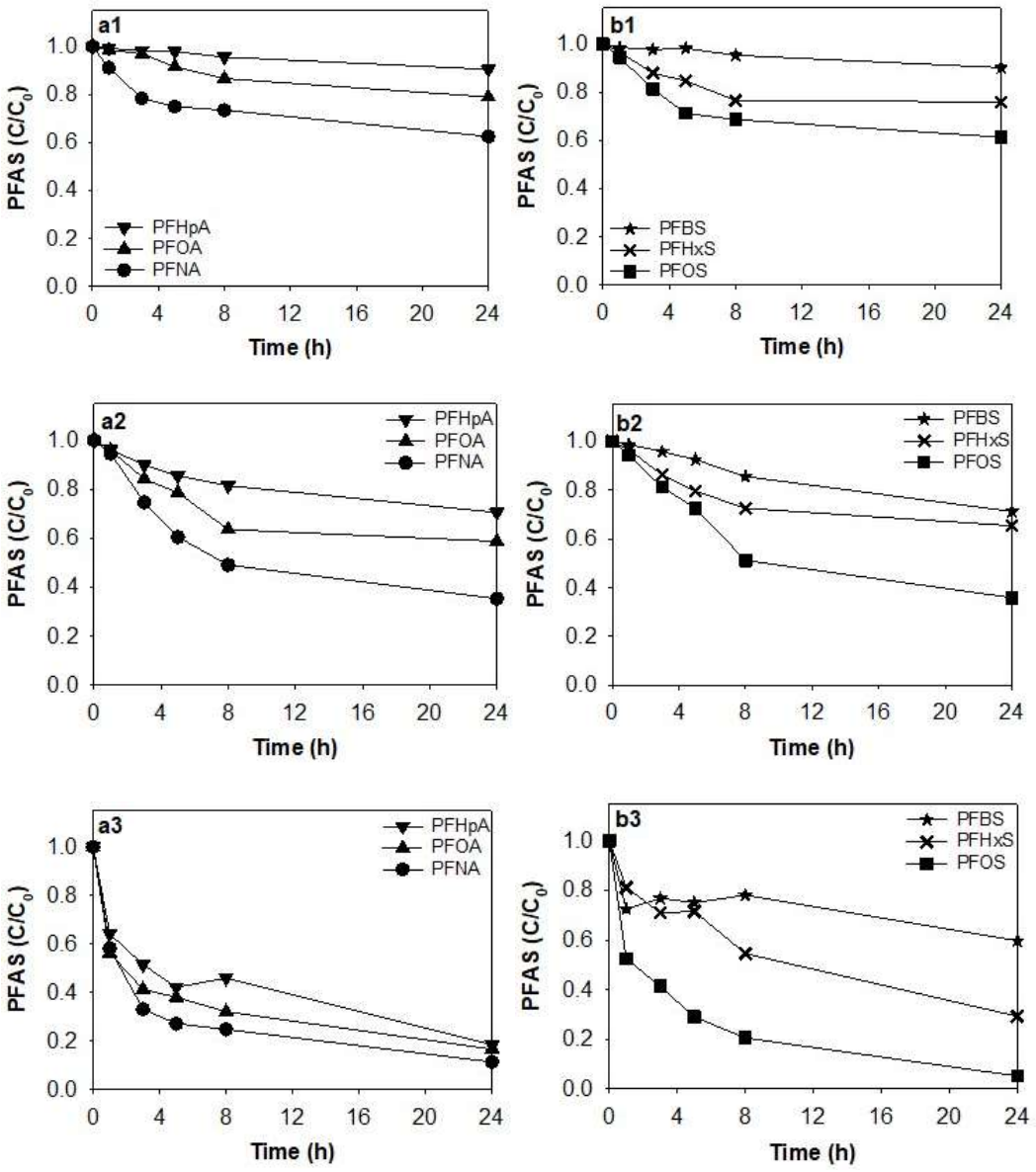

Figure 4-11:Removal of aqueous (a) carboxylic PFAS and (b) sulfonic PFAS in water by RAC conjugated with PS at (1) 20 ℃, (2) 40 ℃, and (3) 60 ℃ (10 mg/L PFAS; 20 g/L RAC; no soil; 0.3 M PS; 20-60 ℃; 1 atm; and initial pH around 9 to final pH around 2 (no pH control).

Third, although higher temperatures showed more removal of PFAS and SRs are capable to decompose PFSA, no identifiable byproducts were identified at 20 ℃ either in the aqueous or solid phase and negligible amounts of byproducts were also found at 40 ℃ (Lei et al., 2020), suggesting that removal mechanism of PFAS even in the presence of PS at 20 ℃ and 40 ℃ might be adsorption. Along with higher temperatures, the presence of PS accelerated oxidation of ZVI to Fe oxides and Fe hydroxides with high affinity for PFAS, which was supported by fast colour change of the reaction solution to reddish brown (Parenky et al., 2020; Park, Zenobio, and Lee, 2018). Importantly, only the case of RAC in the presence of PS at 60 ℃ exhibited reaction byproducts.

4.5 Evolution of reaction byproduct

Reaction temperature seems to be the most important factor to decompose PFAS by producing reactive radicals and accelerating reaction kinetics. Heat-activated PS has been known to be effective to produce SRs at high temperature of at least 60-90 ℃ (Park et al., 2016; Lee et al., 2013; Liu et al., 2012). However, only carboxylic PFAS were removed via physical adsorption combined with chemical decomposition, while no significant byproducts were identified from sulfonic PFAS and thus they were removed via adsorption mechanism. Identifiable aqueous byproducts formed during decomposition of PFNA, PFOA, and PFHpA by RAC conjugated with PS at 60 ℃ was traced via targeted LC/MS analysis. Formation of short chain PFAS was obvious, as shown in Fig. 4-12. Evolution of the limited byproducts over time is shown in Fig.4-13. Decomposition of PFNA (C9) led to formation of PFOA (C8), PFHpA (C7), perfluorohexanoic acid (PFHxA, C6), perfluoropentanoic acid (PFPeA, C5), and perfluorobutanoic acid (PFBA, C4). Similarly, decomposition of PFOA and PFHpA led to the formation of subsequent short chain PFAS byproducts.

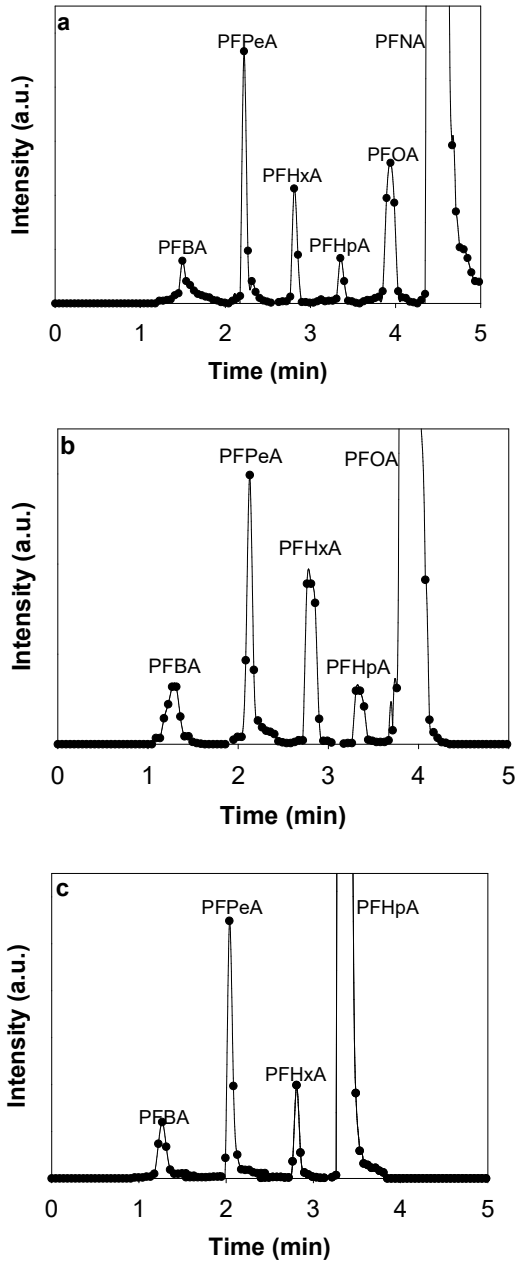

Figure 4-12: LC/MS chromatogram based on targeted analysis, showing identifiable aqueous byproducts formed during decomposition of parent PFAS: (a) PFNA, (b) PFOA, and (c) PFHpA in water by RAC conjugated with PS at 60 ℃ (10 mg/L PFAS; 20 g/L RAC; no soil, 0.3 M PS; 60 ℃; 1 atm; and initial pH around 9 to final pH around 2 (no pH control)).

Previous studies employing energy-intensive technologies have reported the formation of shorter chain carboxylic PFAS during decomposition of both carboxylic PFAS and sulfonic PFAS (Park et al., 2016; Gu et al., 2017). As proposed by Hori et al. (2010), the main mechanism for the observed decomposition of carboxylic PFAS involves gradual removal of CF_2 moieties and re-formation of a carboxylic functional group on the perfluoroalkyl radical through a series of radical reactions. Significant removal of carboxylic PFAS, e.g., PFOA at 83% (from 10 mg/L to around 1.7 mg/L) was observed in 24 h while total identifiable aqueous byproducts (i.e., sum of C4-C7) accounted for only 0.24% (around 0.024 mg/L), implying that the difference can be ascribed to mainly adsorption of PFOA and partly formation of many other ill-defined byproducts, strong adsorption of byproducts, and possibly mineralization of PFOA (Parenky et al., 2020). Low levels of fluoride ions were detected at around 0.01-0.2 mg/L after 24 h, suggesting reductive defluorination and/or mineralization of PFAS were not so significant. Alternatively, released fluoride ions could have been removed from water via quick adsorption onto solid surface and/or formation of hydrofluoric acid under such acidic condition.

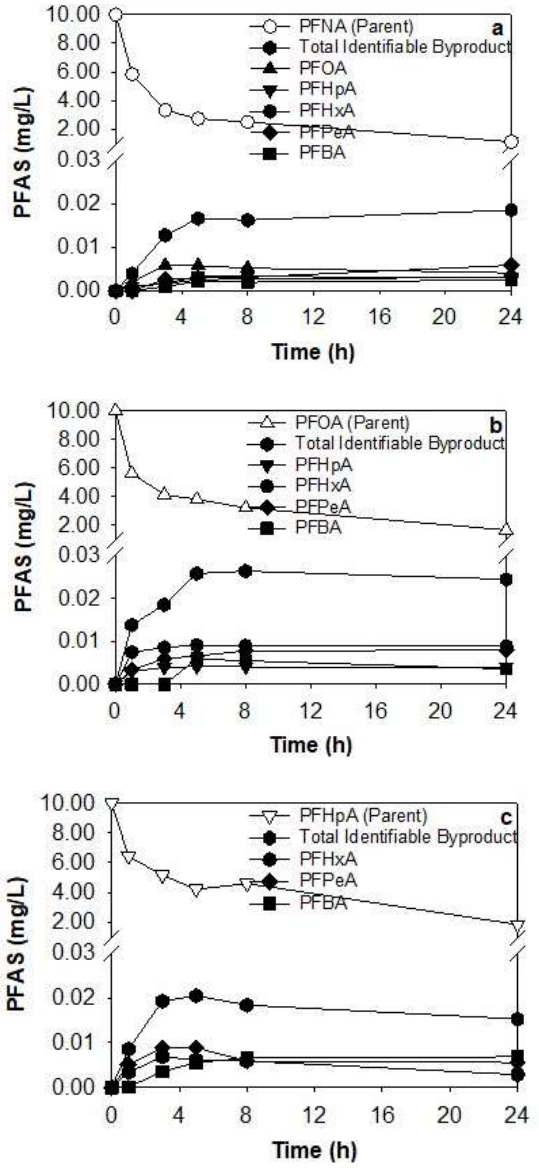

Figure 4-13: Figure 6. Evolution of identifiable aqueous byproducts formed during decomposition of parent PFAS: (a) PFNA, (b) PFOA, and (c) PFHpA in water by RAC conjugated with PS at 60 ℃ (10 mg/L PFAS; 20 g/L RAC; no soil, 0.3 M PS; 60 ℃; 1 atm; and initial pH around 9 to final pH around 2 (no pH control)). Please note total identifiable byproducts count for only the limited number of short-chain PFAS byproducts (e.g., 5 for PFNA) among innumerable ill-defined byproducts.

4.6 Removal of PFAS in water and soil slurry by RAC conjugated with oxidant

PFAS are generally present in complex media rather than in pure aqueous media. In particular, soil particles containing organic matter may greatly influence the chemical reaction of PFAS with RAC. Since only RAC conjugated with PS at 60 ℃ showed decomposition of PFAS in water, the same experiments were conducted in the presence of soil at 20 g/L. Removal of aqueous PFAS in water and soil slurry is shown in Fig. 4-14 and evolution of identifiable aqueous byproducts is shown in Fig. 4-15, which are comparable to Figs. 4-11(a3) and 4-11(b3), and Fig. 4-13 conducted in water, respectively.

Although overall removal kinetics followed the same trends (note Figs. 4-11(a3) and 4-11(b3) in water vs. Figs. 4-14(a) and 4-14(b) in slurry), removal was marginally improved in water and soil slurry most likely due to the presence of more sorbent materials. PFAS have high affinity for soils, particularly clays, and interact with them through similar mechanisms involved in adsorption to GAC, i.e., hydrophobic adsorption, which is dominant with increasing alkyl chain length (Sorengard, Kleja, and Ahrens, 2019).

In addition, organic matter in soils may affect PFAS sorption to RAC negatively but to itself positively (Kothawala et al., 2017; Rayne and Forest, 2009). Even in this case, only carboxylic PFAS were decomposed. The presence of soil seemed to slightly reduce the reactivity of RAC (note Fig. 6 for water vs. Fig. 8 for slurry). Total identifiable aqueous byproducts were decreased from 0.019 mg/L to 0.013 mg/L for PFNA (32% reduction) and from 0.024 mg/L to 0.016 mg/L for PFOA (33% reduction) but increased from 0.015 mg/L to 0.021 mg/L for PFHpA (40% increase).

Organic matter and ionic species in soils may quench reactive species produced from RAC conjugated with PS (Park et al., 2016). Fluoride ions were found at 0.01-0.1

mg/L, slightly less than that observed in the case without soil. Overall, however, the presence of soil particles did not significantly affect removal of PFAS.

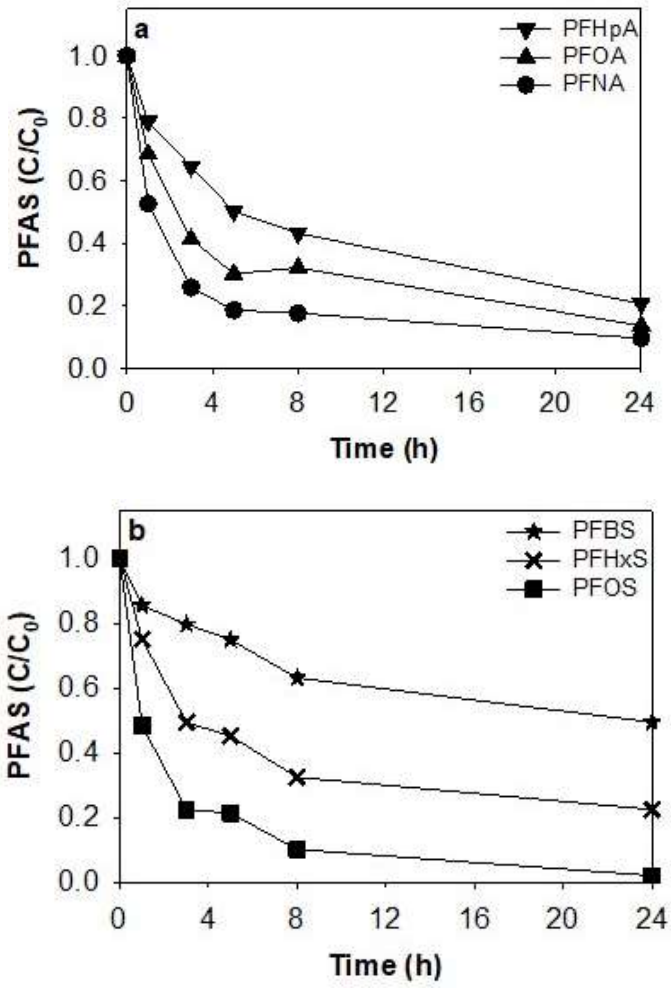

Figure 4-14: Removal of aqueous (a) carboxylic PFAS and (b) sulfonic PFAS in water and soil slurry by RAC conjugated with PS at 60 ℃ (10 mg/L PFAS; 20 g/L RAC; 20 g/L soil; 0.3 M PS; 60 ℃; 1 atm; and initial pH around 9 to final pH around 2 (no pH control)).

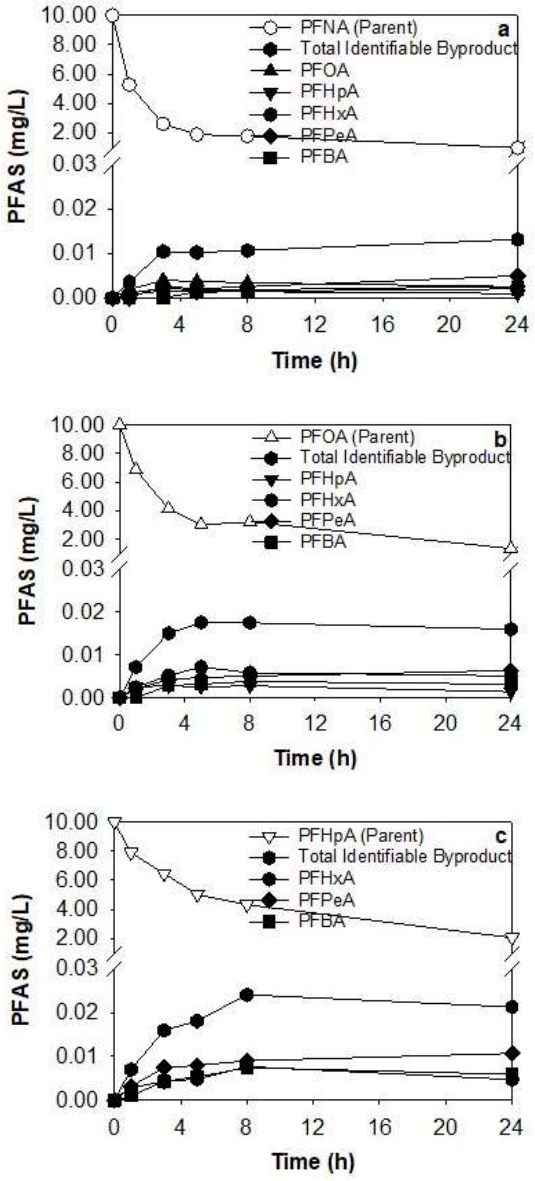

Figure 4-15: Evolution of identifiable aqueous byproducts formed during decomposition of parent PFAS: (a) PFNA, (b) PFOA, and (c) PFHpA in water and soil slurry by RAC conjugated with PS at 60 ℃ (10 mg/L PFAS; 20 g/L RAC; 20 g/L soil, 0.3 M PS; 60 ℃; 1 atm; and initial pH around 9 to final pH around 2 (no pH control)). Please note total identifiable byproducts count for only the limited number of short-chain PFAS byproducts (e.g., 5 for PFNA) among innumerable ill-defined byproducts.

4.8 Impact of iron on the system

In order to understand the impact of the addition of iron on the reaction, a carboxylic (PFOA) and a sulfonic (PFOS) PFAS were evaluated for aqueous removal under the higher temperature studied (60 ℃), which has shown the greater decomposition capacity.

As shown in Fig. 4-16, the removal by GAC alone presents the greater efficiency when compared to all other conditions in the case of both PFOA and PFOS. However, the greatest difference can be observed in the case of PS alone which does not impact PFOS removal but significantly removes PFOA. PFOA removal by PS alone is ascribed to decomposition due to the lack of sorbent and the significant production of byproducts. In the case of PFOS when injected with PS and ZVI, significant removal was observed despite the lack of decomposition indication (F^- release, byproduct formation). The removal in this case has been ascribed to adsorption onto solid particles and complexation with aqueous, oxidized iron particles (Parenky et. al, 2020). In fact, in all condition tested for PFOS, there was no indication of degradation suggesting sorption was the main mechanism for removal in heterogeneous systems. In the case of PFOS, the addition of iron to the system aids removal in the case of PS + ZVI, but hinders removal in the case of RAC versus GAC (both with or without PS) probably due to the reduction in the pore volume and sorption area of the base material.

In contrast, PFOA decomposition was confirmed in all systems under these conditions except for GAC alone. The greater removal observed in the case of GAC and GAC + PS versus RAC and RAC + PS is expected due to the greater surface area of GAC. The greater removal of PFOA by PS alone suggests that the main decomposition pathway occurs through heat-activated persulfate as opposed to the activation of PS by transition

metal. An appropriate ratio of oxidant to metal has been shown to be determinant to the proper activation of the oxidant and radical production otherwise there is quenching of the radicals by the metal ions (Nfodzo and Choi, 2011).

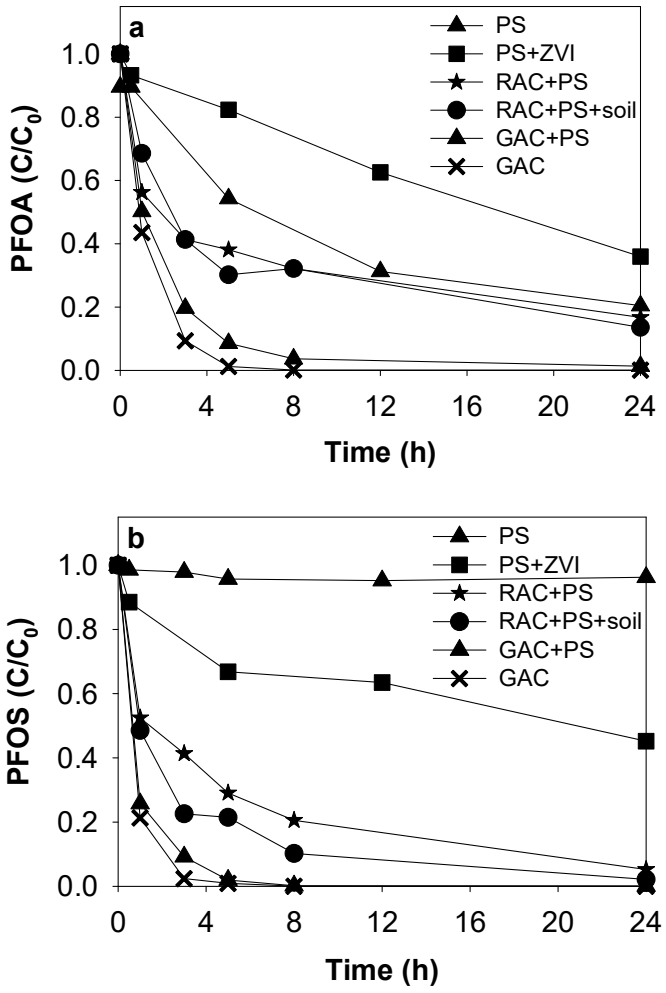

Figure 4-16: Removal of aqueous (a) PFOA and (b) PFOS by PS alone and PS conjugated with ZVI, GAC and GAC conjugated with PS, RAC, RAC conjugated with PS and soil RAC slurry conjugated with PS (10 mg/L PFAS; 20 g/L RAC; 20g/L GAC, 20 g/L soil, 0.3 M PS; 60 ℃; 1 atm).

4.7 Partitioning of PFAS and byproducts

During reaction, PFAS are adsorbed and partitioned into the aqueous phase, RAC solid phase and/or soil phase, and then, if any, they are decomposed to produce various reaction byproducts, which are also re-partitioned into the three phases, as depicted in Fig. 4-17. Some of PFAS and byproducts may go to complete mineralization to H_2O and CO_2.

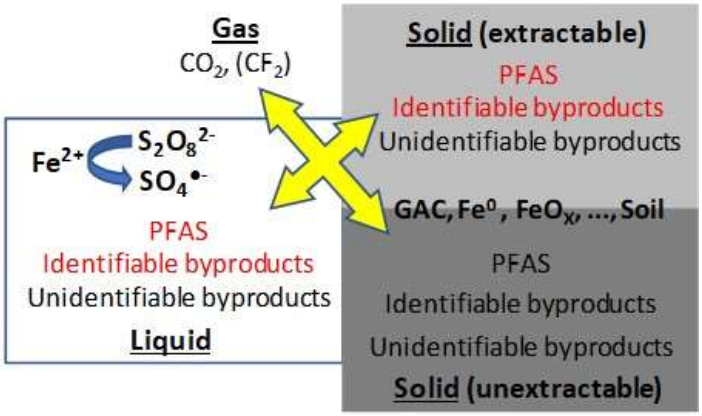

Figure 4-17: Partitioning of PFAS and byproducts into the liquid, solid, and gas phases. Carbon mass balance can be set only based on observed PFAS and byproducts (highlighted with red). Please note that the number of identifiable byproducts (only a few to several) is overwhelmed by that of unidentifiable byproducts.

Since it is hard to qualify and quantify all byproducts, recover all PFAS and byproducts from the solid phases, and precisely measure total mineralization in this heterogeneous system, setting up accurate PFAS carbon mass balance is impossible. As a result, based on solely the observed results, partitioning of parent PFAS and identifiable byproducts to the aqueous phase and solid phase is summarized in Fig. 4-18.

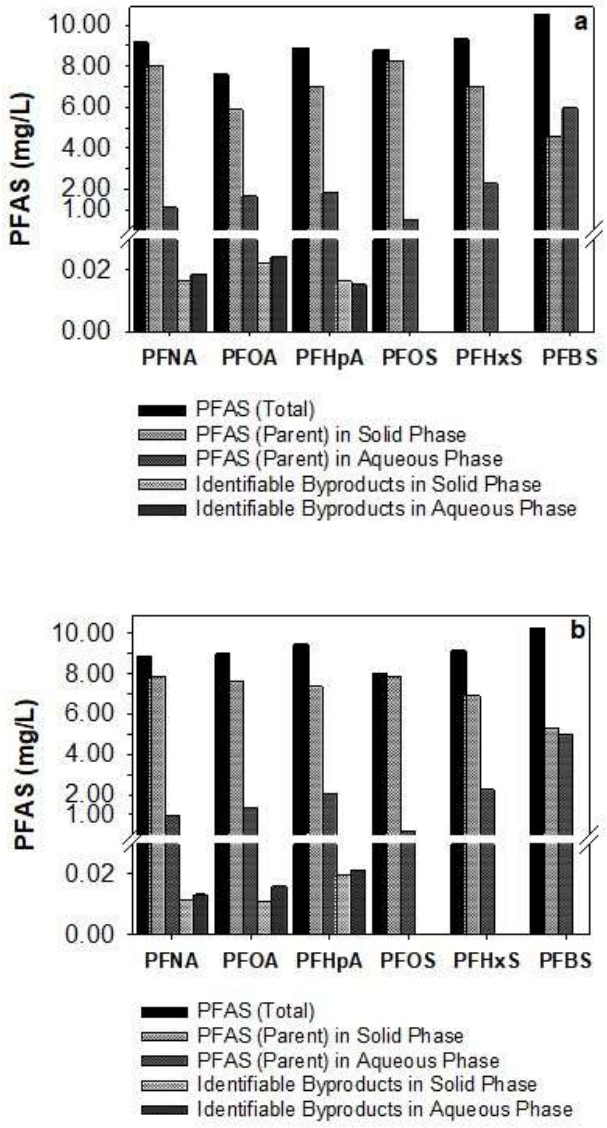

Figure 4-18: Partitioning of parent PFAS and identifiable byproducts to the aqueous phase and solid phase (i.e., RAC in (a) and RAC and soil (b)) after 24 h reaction of PFAS in (a) water and (b) water and soil slurry with RAC conjugated with PS at 60 ℃ (10 mg/L PFAS; 20 g/L RAC; no soil and 20g/L soil, 0.3 M PS; 60 ℃; 1 atm; and initial pH around 9 to final pH around 2 (no pH control)). Total PFAS represents the sum of all detected parent and byproduct PFAS in the reactor, in comparison to initial PFAS at 10 mg/L.

Total PFAS observed was very similar or slightly less than initial PFAS at 10 m/L (0-24% less). The difference can be considered as unrecovered PFAS, which is ascribed more likely to formation of ill-defined byproducts which were unidentifiable through the targeted analysis used in this study, presence of unextractable parent and byproduct PFAS from the solid phase, and less likely mineralization of PFAS to CO_2. Most of parent PFAS stayed adsorbed onto the solid phase of either RAC or soil while small amounts of PFAS were decomposed. Although it is not clear if the decomposition occurred mainly in the solid phase or in the aqueous phase, identifiable byproducts were partitioned almost equally into the aqueous and solid phases. Interestingly, formation of identifiable byproducts was stopped in around 3-8 h (note Figs. 6 and 8). These results suggest a need of accelerating decomposition kinetics by modifying the system, such as intermittent injection of smaller amounts of PS and use of transition metals other than Fe.

It should also be noted that amounts of total identifiable byproducts in the aqueous and solid phases were very low because they account for only the limited number of short chain PFAS byproducts (e.g., 5 for PFNA, 4 for PFOA, and 3 for PFHpA) among innumerable ill-defined byproducts. Measurement of total organic carbon (TOC) reduction was once considered but not conducted because TOC removal does not necessarily represent mineralization in this case. In this heterogeneous system, TOC level in water can also be reduced mainly by PFAS adsorption and affected by organic matter originated from GAC. Nonetheless, the obvious formation of the identifiable short chain PFAS byproducts (Figs. 5, 6, and 8) and the presence of various peaks in the chromatogram indicate presumably more significant decomposition of PFAS.

Many previous studies demonstrated the effect of the structural properties of PFAS on their adsorption tendency onto solid materials (Rayne and Forest, 2009; Yu et al., 2009; Gagliano et al., 2020; Zhao et al., 2014). Adsorbents become more hydrophobic over initial

adsorption of PFAS, and thus two different adsorption kinetics can be (McCleaf et al., 2017; Lawal and Choi, 2018). Adsorption of PFAS is also greatly affected by ionic strength and pH of reaction solution and the presence of organic matter and soil particle (Kothawala et al., 2017; Zhang, Zhang, and Liang, 2019; Kah et al., 2017; Milinovic et al., 2015). Additionally, ZVI, along with GAC as a base adsorbent, also involves in adsorption of PFAS and byproducts. Most importantly, radical species generated under certain conditions such as PS at 60 ℃ attack and decompose PFAS and quickly oxidize ZVI into Fe oxides and Fe hydroxides, which also show great affinity for PFAS as well as possibly byproducts (Parenky et al., 2020; Park, Zenobio, and Lee, 2018).

Chapter 5

Conclusions and Future Recommendations

The potential of GAC impregnated with ZVI nanoparticles to implement adsorption-mediated chemical decomposition of PFAS in the presence of an oxidant PS was demonstrated. The mesoporous GAC selected to place ZVI particles was proven to adsorb the 6 PFAS tested in order of PFNA>PFOS>PFHpA>PFHxS>PFOA>PFBS. Regardless of the presence of PS, higher temperature, longer chain PFAS, and sulfonic PFAS were more favourable for PFAS removal kinetics than the counter parts. RAC conjugated with PS at 60 ℃ exhibited decomposition of PFAS, exclusively carboxylic PFAS, obviously producing various identifiable short chain PFAS. Carboxylic PFAS were removed via physical adsorption combined with chemical decomposition while sulfonic PFAS were removed solely via adsorption mechanism. The presence of soil did not greatly affect the overall removal of PFAS. Carbon mass balance suggested that PFAS decomposition and ZVI oxidation by radical mechanisms mutually influence, in a complex manner, PFAS adsorption event to GAC, ZVI and its derivatives, and soil particles. Nonetheless, all tested 6 PFAS were removed significantly. However, the role of ZVI for the chemical reaction is not clear and decomposition of sulfonic PFAS are still challenging. While some of the tested PFAS were decomposed, future studies should investigate combinations of many other oxidants and transition metals other than ZVI at/in different oxidation states/groups to over the requirement of heat and decompose sulfonic PFAS. Additionally, a solution mixture of PFAS should be tested to identify the possibility of competition amongst the PFAS for adsorption and decomposition. Column tests of the selected system should also be carried to simulate the real working adsorption bed and understand breakthrough of the modified system.

Appendix A

Mass-labelled Isotopes Present in Internal Standard Solution

Table A-1 Mass labeled isotopes utilized as a mixture for extraction and injection standards.

Mass-labelled isotopes present in extraction standard solution (2 000 ng/mL each)	
Perfluorinated Compound	Abbreviation
Perfluoro-n-[$^{13}C_4$]butanoic acid	MPFBA
Perfluoro-n-[$^{13}C_5$]pentanoic acid	M5PFPeA
Perfluoro-n-[1,2,3,4,6-$^{13}C_5$]hexanoic acid	M5PFHxA
Perfluoro-n-[1,2,3,4-$^{13}C_4$]heptanoic acid	M4PFHpA
Perfluoro-n-[$^{13}C_8$]octanoic acid	M8PFOA
Perfluoro-n-[$^{13}C_9$]nonanoic acid	M9PFNA
Perfluoro-n-[1,2,3,4,5,6-$^{13}C_6$]decanoic acid	M6PFDA
Perfluoro-n-[1,2,3,4,5,6,7-$^{13}C_7$]undecanoic acid	M7PFUdA
Perfluoro-n-[1,2-$^{13}C_2$]dodecanoic acid	MPFDoA
Perfluoro-n-[1,2-$^{13}C_2$]tetradecanoic acid	M2PFTeDA
Sodium perfluoro-1-[2,3,4-$^{13}C_3$]butanesulfonate	M3PFBS
Sodium perfluoro-1-[1,2,3-$^{13}C_3$]hexanesulfonate	M3PFHxS
Sodium perfluoro-1-[2,3,4-$^{13}C_3$]octanesulfonate	M8PFOS
Mass-labelled isotopes present in injection standard solution (2 000 ng/mL each)	
Perfluoro-n-[2,3,4-$^{13}C_3$]butanoic acid	M3PFBA
Perfluoro-n-[1,2-$^{13}C_2$]octanoic acid	M2PFOA
Perfluoro-n-[1,2-$^{13}C_2$]decanoic acid	MPFDA
Sodium perfluoro-1-[1,2,3,4-$^{13}C_4$]octanesulfonate	MPFOS

Appendix B

Precursor Ion and Mass to Charge Ratios of Targeted PFAS

Table B-1 Precursor ions of targeted PFAS evaluated through LC-MS/MS.

Analyte	Precursor ion	Product ion (Quantitative)	Product ion (Qualitative)	Ionization mode
PFOA	413	369	169	negative
PFOS	499	80	99	negative
PFNA	463	419	219	negative
PFHpA	363	319	169	negative
PFHxS	399	80	99	negative
PFBS	299	80	99	negative

Appendix C

Porosimetry Analysis of GAC

Full Report Set

Sample: 2018 09 05 3000 GAC raw
Operator: Pasouza
Submitter:
File: C:\TriStar II 3020\data...\2018 09 05 3000 GAC raw.SMP

Started:	9/5/2018 3:53:22 PM	Analysis Adsorptive:	N2
Completed:	9/6/2018 8:27:56 AM	Analysis Bath Temp.:	-195.800 °C
Report Time:	9/6/2018 3:01:37 PM	Thermal Correction:	No
Sample Mass:	0.2678 g	Warm Free Space:	9.6028 cm³ Measured
Cold Free Space:	29.4888 cm³	Equilibration Interval:	5 s
Low Pressure Dose:	None	Sample Density:	1.000 g/cm³
Automatic Degas:	No		

Summary Report

Surface Area

Single point surface area at P/Po = 0.299182205: 590.3430 m²/g

BET Surface Area: 593.1701 m²/g

BJH Adsorption cumulative surface area of pores between 17.000 Å and 3,000.000 Å diameter: 110.745 m²/g

BJH Desorption cumulative surface area of pores between 17.000 Å and 3,000.000 Å diameter: 194.0684 m²/g

Pore Volume

Single point adsorption total pore volume of pores less than 4.445 Å diameter at P/Po = 0.010000000: 0.207382 cm³/g

BJH Adsorption cumulative volume of pores between 17.000 Å and 3,000.000 Å diameter: 0.217170 cm³/g

BJH Desorption cumulative volume of pores between 17.000 Å and 3,000.000 Å diameter: 0.261940 cm³/g

Pore Size

Adsorption average pore diameter (4V/A by BET): 13.9846 Å

BJH Adsorption average pore diameter (4V/A): 78.439 Å

BJH Desorption average pore diameter (4V/A): 53.989 Å

Sample: 2018 09 05 3000 GAC raw
Operator: Pasouza
Submitter:
File: C:\TriStar II 3020\data...\2018 09 05 3000 GAC raw.SMP

Started:	9/5/2018 3:53:22 PM	Analysis Adsorptive:	N2
Completed:	9/6/2018 8:27:56 AM	Analysis Bath Temp.:	-195.800 °C
Report Time:	9/6/2018 3:01:37 PM	Thermal Correction:	No
Sample Mass:	0.2678 g	Warm Free Space:	9.6028 cm³ Measured
Cold Free Space:	29.4888 cm³	Equilibration Interval:	5 s
Low Pressure Dose:	None	Sample Density:	1.000 g/cm³
Automatic Degas:	No		

Isotherm Linear Plot

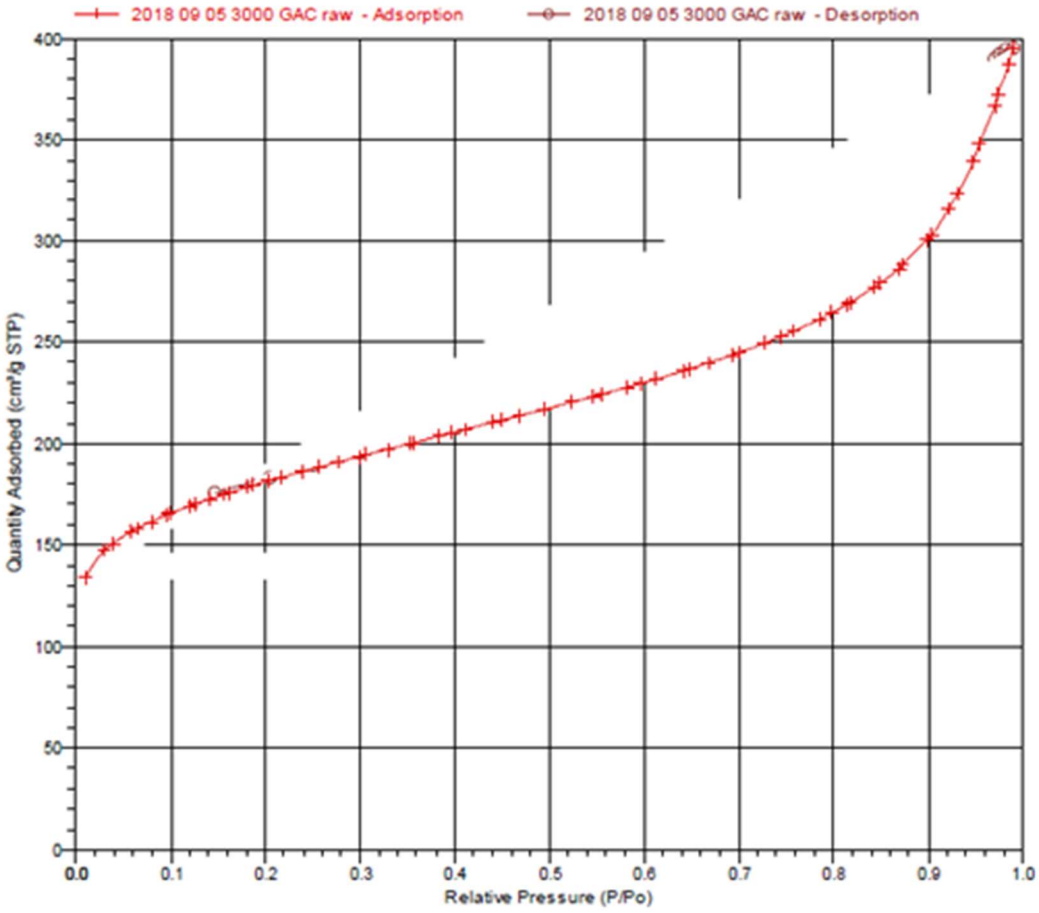

Sample: 2018 09 05 3000 GAC raw
Operator: Pasouza
Submitter:
File: C:\TriStar II 3020\data...\2018 09 05 3000 GAC raw.SMP

Started:	9/5/2018 3:53:22 PM	Analysis Adsorptive:	N2
Completed:	9/6/2018 8:27:56 AM	Analysis Bath Temp.:	-195.800 °C
Report Time:	9/6/2018 3:01:37 PM	Thermal Correction:	No
Sample Mass:	0.2678 g	Warm Free Space:	9.6028 cm³ Measured
Cold Free Space:	29.4888 cm³	Equilibration Interval:	5 s
Low Pressure Dose:	None	Sample Density:	1.000 g/cm³
Automatic Degas:	No		

BET Surface Area Plot

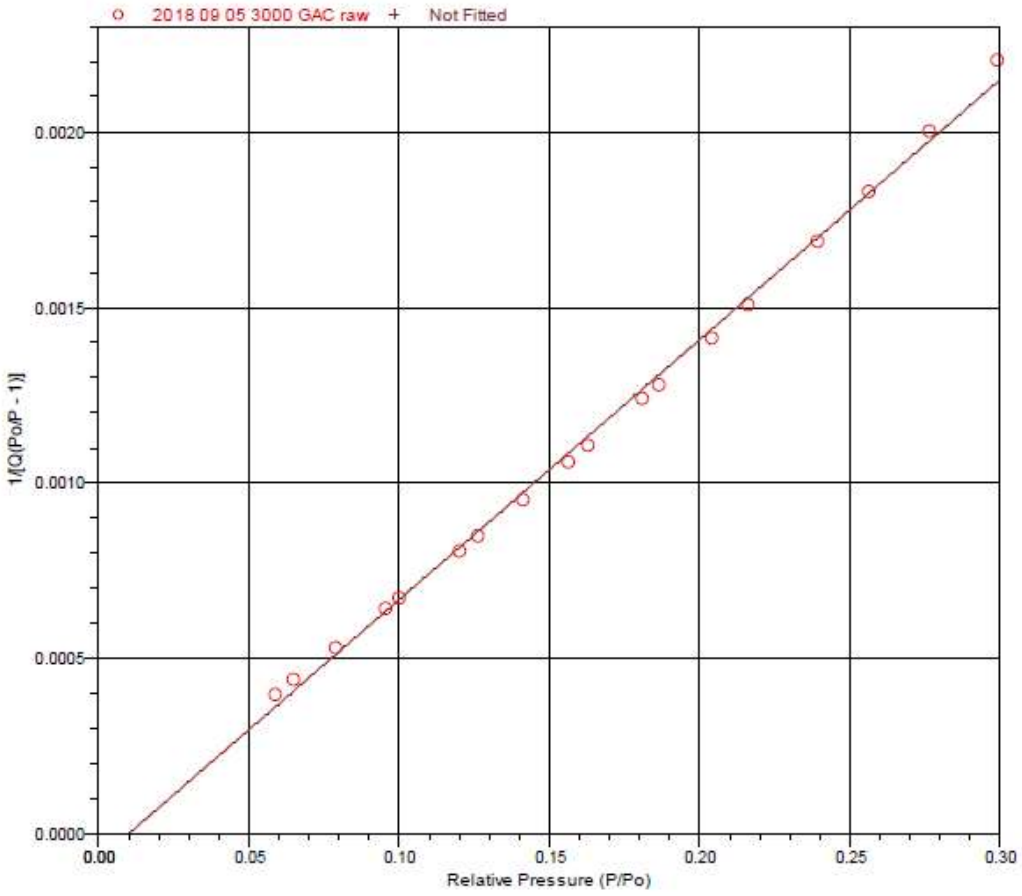

Sample: 2018 09 05 3000 GAC raw
Operator: Pasouza
Submitter:
File: C:\TriStar II 3020\data...\2018 09 05 3000 GAC raw.SMP

Started:	9/5/2018 3:53:22 PM	Analysis Adsorptive:	N2
Completed:	9/6/2018 8:27:56 AM	Analysis Bath Temp.:	-195.800 °C
Report Time:	9/6/2018 3:01:37 PM	Thermal Correction:	No
Sample Mass:	0.2678 g	Warm Free Space:	9.6028 cm³ Measured
Cold Free Space:	29.4888 cm³	Equilibration Interval:	5 s
Low Pressure Dose:	None	Sample Density:	1.000 g/cm³
Automatic Degas:	No		

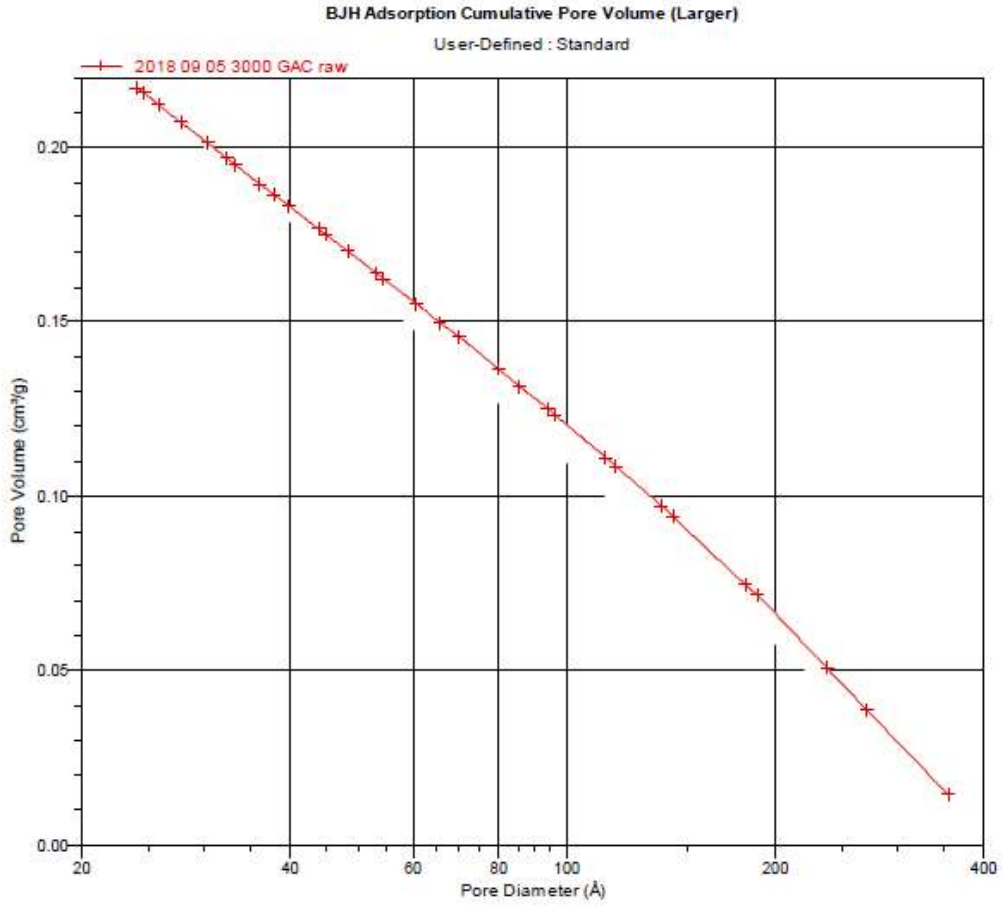

Sample: 2018 09 05 3000 GAC raw
Operator: Pasouza
Submitter:
File: C:\TriStar II 3020\data...\2018 09 05 3000 GAC raw.SMP

Started:	9/5/2018 3:53:22 PM	Analysis Adsorptive:	N2
Completed:	9/6/2018 8:27:56 AM	Analysis Bath Temp.:	-195.800 °C
Report Time:	9/6/2018 3:01:37 PM	Thermal Correction:	No
Sample Mass:	0.2678 g	Warm Free Space:	9.6028 cm³ Measured
Cold Free Space:	29.4888 cm³	Equilibration Interval:	5 s
Low Pressure Dose:	None	Sample Density:	1.000 g/cm³
Automatic Degas:	No		

BJH Adsorption Cumulative Pore Area (Larger)

User-Defined : Standard

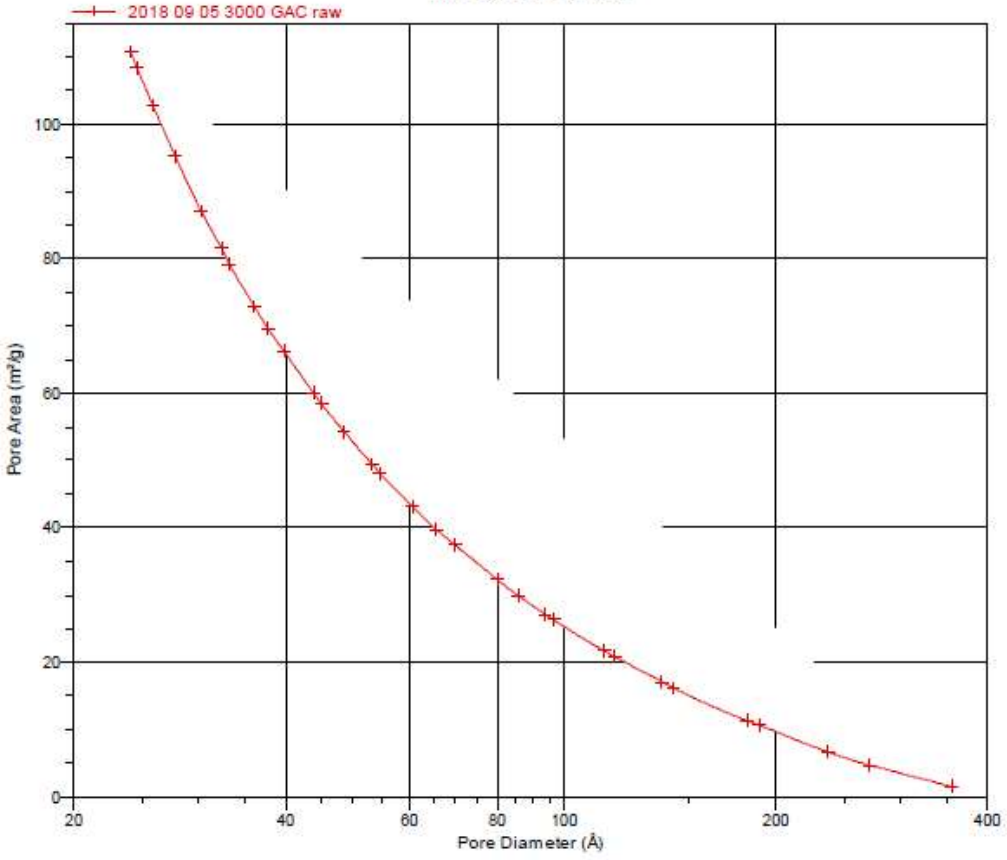

Sample: 2018 09 05 3000 GAC raw
Operator: Pasouza
Submitter:
File: C:\TriStar II 3020\data...\2018 09 05 3000 GAC raw.SMP

Started:	9/5/2018 3:53:22 PM	Analysis Adsorptive:	N2
Completed:	9/6/2018 8:27:56 AM	Analysis Bath Temp.:	-195.800 °C
Report Time:	9/6/2018 3:01:37 PM	Thermal Correction:	No
Sample Mass:	0.2678 g	Warm Free Space:	9.6028 cm³ Measured
Cold Free Space:	29.4888 cm³	Equilibration Interval:	5 s
Low Pressure Dose:	None	Sample Density:	1.000 g/cm³
Automatic Degas:	No		

BJH Desorption Cumulative Pore Volume (Larger)

User-Defined : Standard

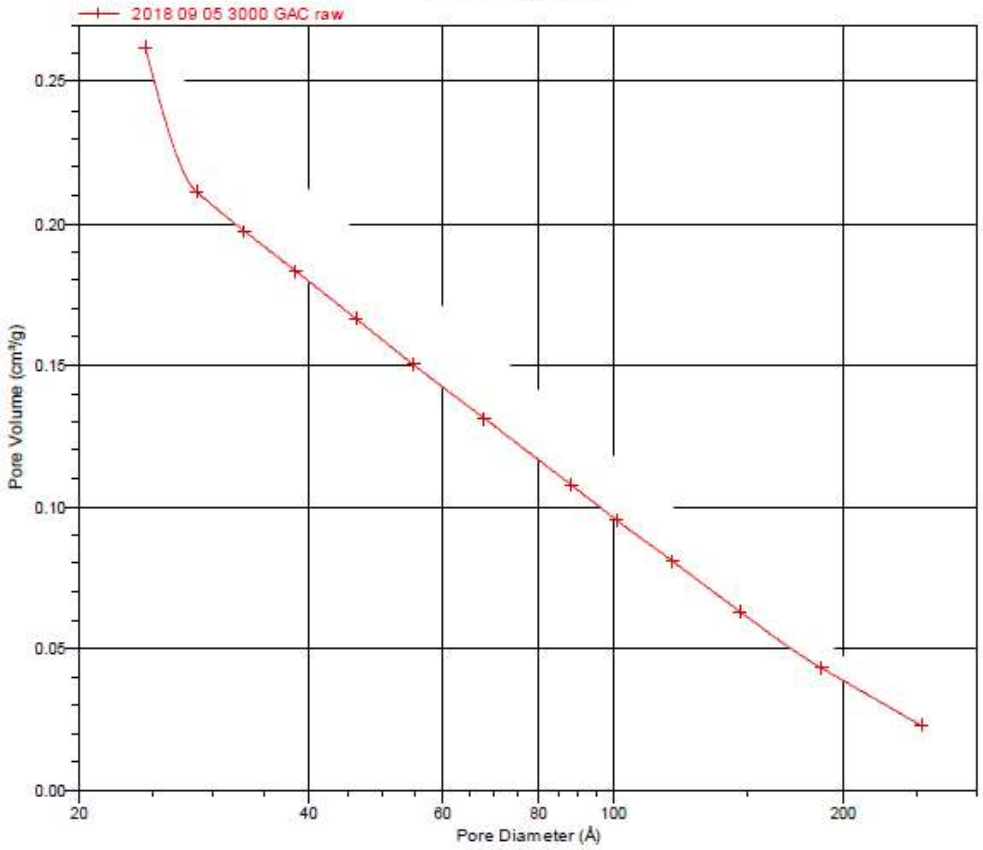

Sample: 2018 09 05 3000 GAC raw
Operator: Pasouza
Submitter:
File: C:\TriStar II 3020\data...\2018 09 05 3000 GAC raw.SMP

Started:	9/5/2018 3:53:22 PM	Analysis Adsorptive:	N2
Completed:	9/6/2018 8:27:56 AM	Analysis Bath Temp.:	-195.800 °C
Report Time:	9/6/2018 3:01:37 PM	Thermal Correction:	No
Sample Mass:	0.2678 g	Warm Free Space:	9.6028 cm³ Measured
Cold Free Space:	29.4888 cm³	Equilibration Interval:	5 s
Low Pressure Dose:	None	Sample Density:	1.000 g/cm³
Automatic Degas:	No		

BJH Desorption Cumulative Pore Area (Larger)

User-Defined : Standard

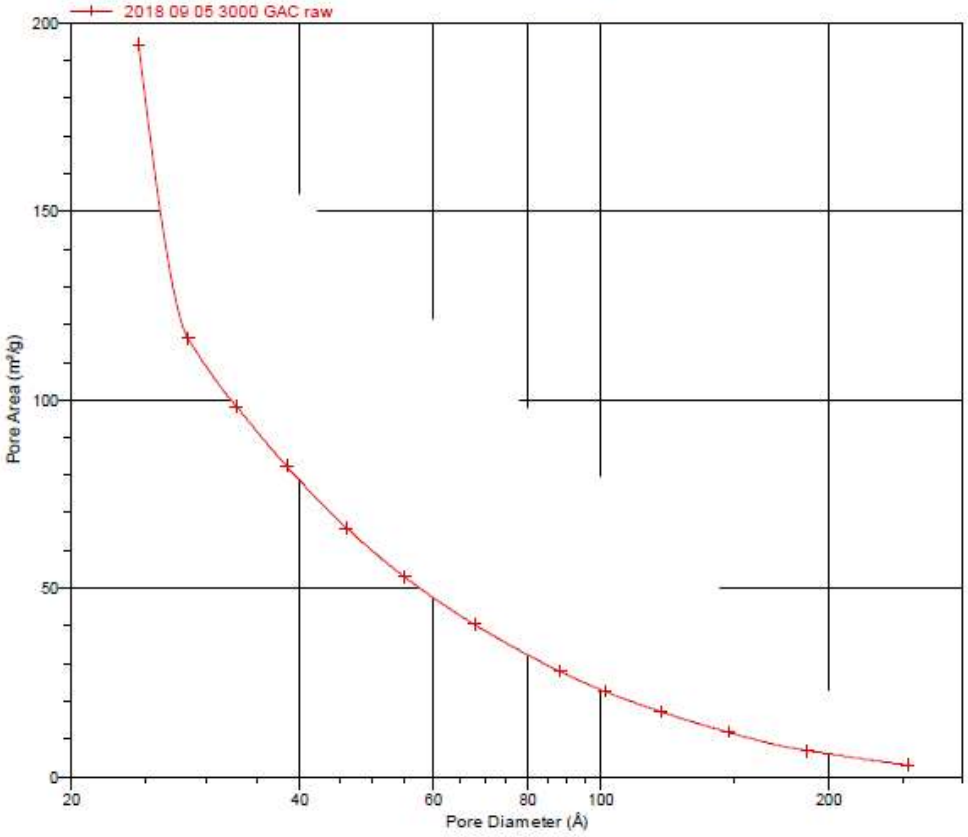

Appendix D

Porosimetry Analysis of RAC

Sample: RAC with etoh and meoh wash
Operator: Akshay
Submitter:
File: C:\TriSt..\2018 10 26 RAC with etoh and meoh wash.SMP

Started:	10/26/2018 10:19:32 AM	Analysis Adsorptive:	N2
Completed:	10/26/2018 8:06:01 PM	Analysis Bath Temp.:	-195.800 °C
Report Time:	10/29/2018 2:53:48 PM	Thermal Correction:	No
Sample Mass:	0.2663 g	Warm Free Space:	9.7221 cm³ Measured
Cold Free Space:	29.2109 cm³	Equilibration Interval:	5 s
Low Pressure Dose:	None	Sample Density:	1.000 g/cm³
Automatic Degas:	No		

Summary Report

Surface Area

Single point surface area at P/Po = 0.297473818:	332.3714 m²/g
BET Surface Area:	336.2433 m²/g
BJH Adsorption cumulative surface area of pores between 17.000 Å and 3,000.000 Å diameter:	66.380 m²/g
BJH Desorption cumulative surface area of pores between 17.000 Å and 3,000.000 Å diameter:	107.3900 m²/g

Pore Volume

Single point adsorption total pore volume of pores less than 4.445 Å diameter at P/Po = 0.010000000:	0.106844 cm³/g
BJH Adsorption cumulative volume of pores between 17.000 Å and 3,000.000 Å diameter:	0.119597 cm³/g
BJH Desorption cumulative volume of pores between 17.000 Å and 3,000.000 Å diameter:	0.136633 cm³/g

Pore Size

Adsorption average pore diameter (4V/A by BET):	12.7104 Å
BJH Adsorption average pore diameter (4V/A):	72.069 Å
BJH Desorption average pore diameter (4V/A):	50.892 Å

Sample: RAC with etoh and meoh wash
Operator: Akshay
Submitter:
File: C:\TriSt...\2018 10 26 RAC with etoh and meoh wash.SMP

Started:	10/26/2018 10:19:32 AM	Analysis Adsorptive:	N2
Completed:	10/26/2018 8:06:01 PM	Analysis Bath Temp.:	-195.800 °C
Report Time:	10/29/2018 2:53:48 PM	Thermal Correction:	No
Sample Mass:	0.2663 g	Warm Free Space:	9.7221 cm³ Measured
Cold Free Space:	29.2109 cm³	Equilibration Interval:	5 s
Low Pressure Dose:	None	Sample Density:	1.000 g/cm³
Automatic Degas:	No		

Isotherm Linear Plot

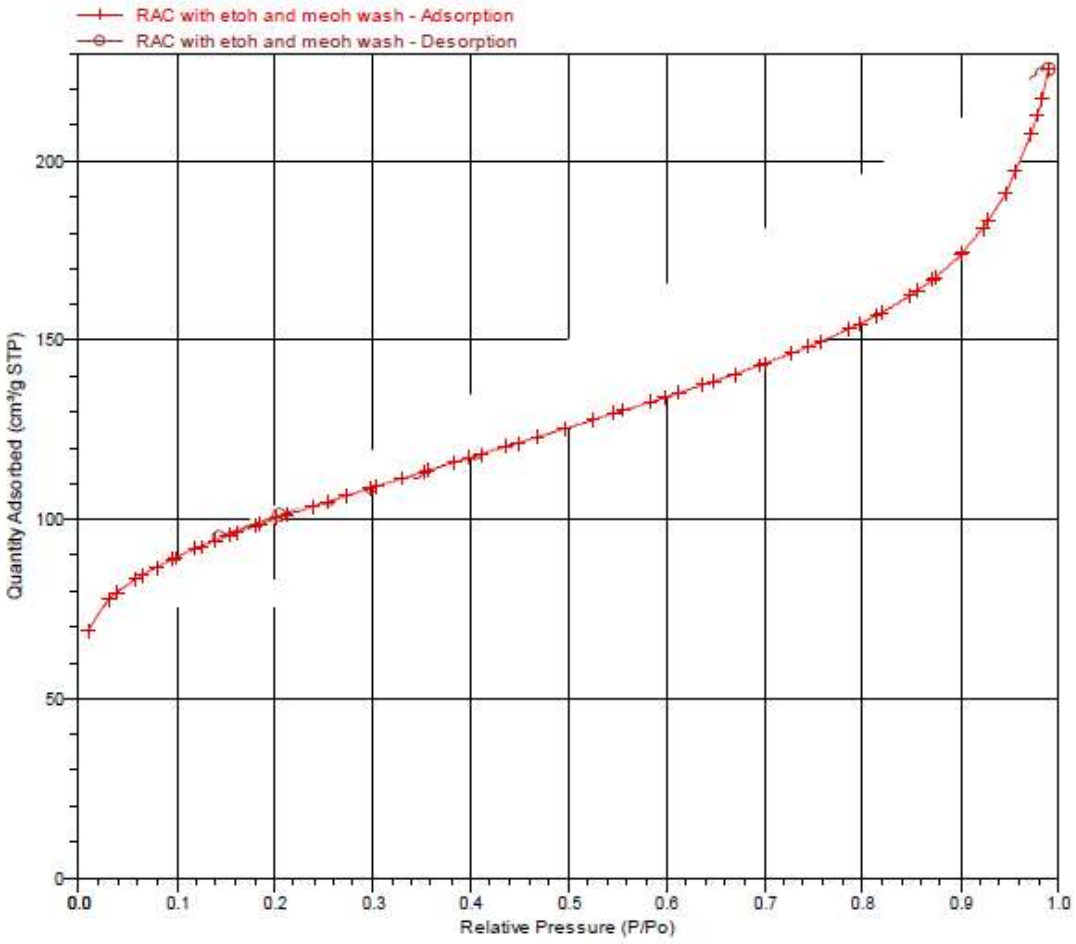

Sample: RAC with etoh and meoh wash
Operator: Akshay
Submitter:
File: C:\TriSt...\2018 10 26 RAC with etoh and meoh wash.SMP

Started:	10/26/2018 10:19:32 AM	Analysis Adsorptive:	N2
Completed:	10/26/2018 8:06:01 PM	Analysis Bath Temp.:	-195.800 °C
Report Time:	10/29/2018 2:53:48 PM	Thermal Correction:	No
Sample Mass:	0.2663 g	Warm Free Space:	9.7221 cm³ Measured
Cold Free Space:	29.2109 cm³	Equilibration Interval:	5 s
Low Pressure Dose:	None	Sample Density:	1.000 g/cm³
Automatic Degas:	No		

BET Surface Area Plot

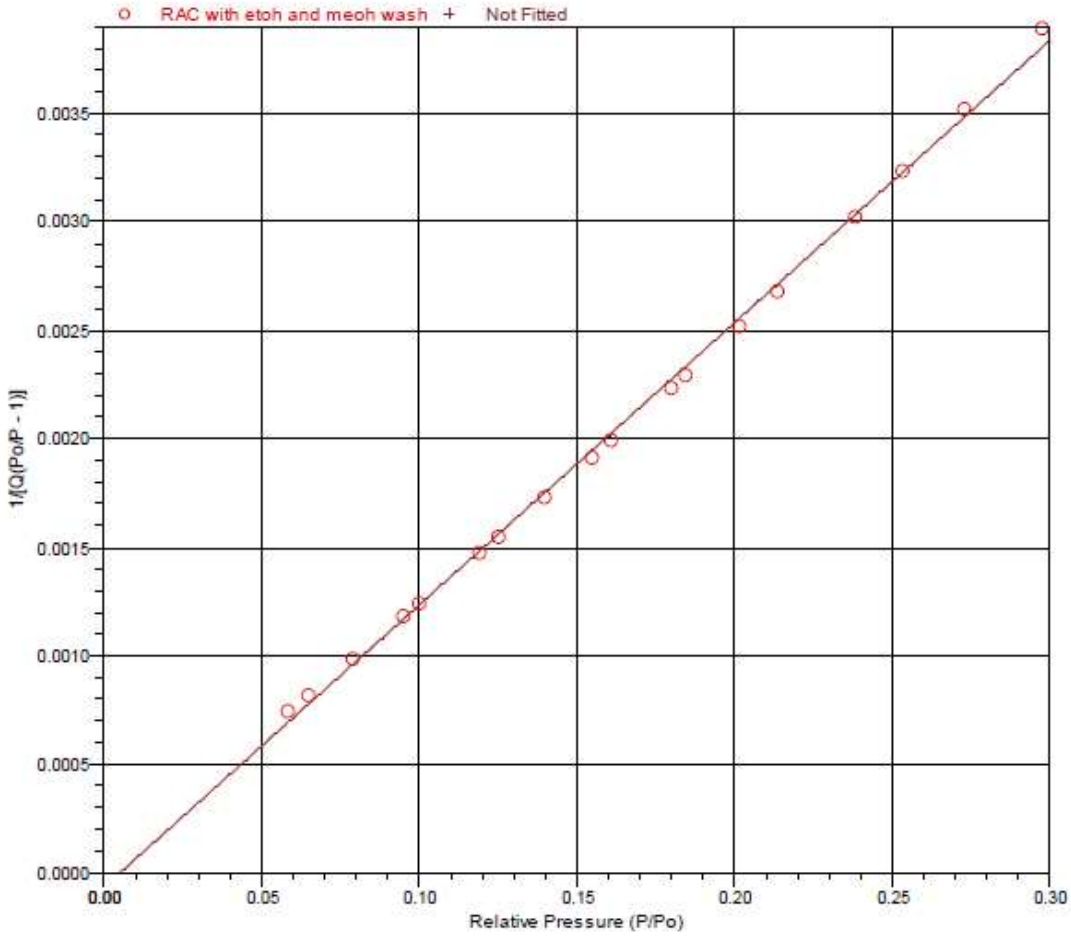

Sample: RAC with etoh and meoh wash
Operator: Akshay
Submitter:
File: C:\TriSt..\2018 10 26 RAC with etoh and meoh wash.SMP

Started:	10/26/2018 10:19:32 AM	Analysis Adsorptive:	N2
Completed:	10/26/2018 8:06:01 PM	Analysis Bath Temp.:	-195.800 °C
Report Time:	10/29/2018 2:53:48 PM	Thermal Correction:	No
Sample Mass:	0.2663 g	Warm Free Space:	9.7221 cm³ Measured
Cold Free Space:	29.2109 cm³	Equilibration Interval:	5 s
Low Pressure Dose:	None	Sample Density:	1.000 g/cm³
Automatic Degas:	No		

BJH Adsorption Cumulative Pore Area (Larger)

User-Defined : Standard

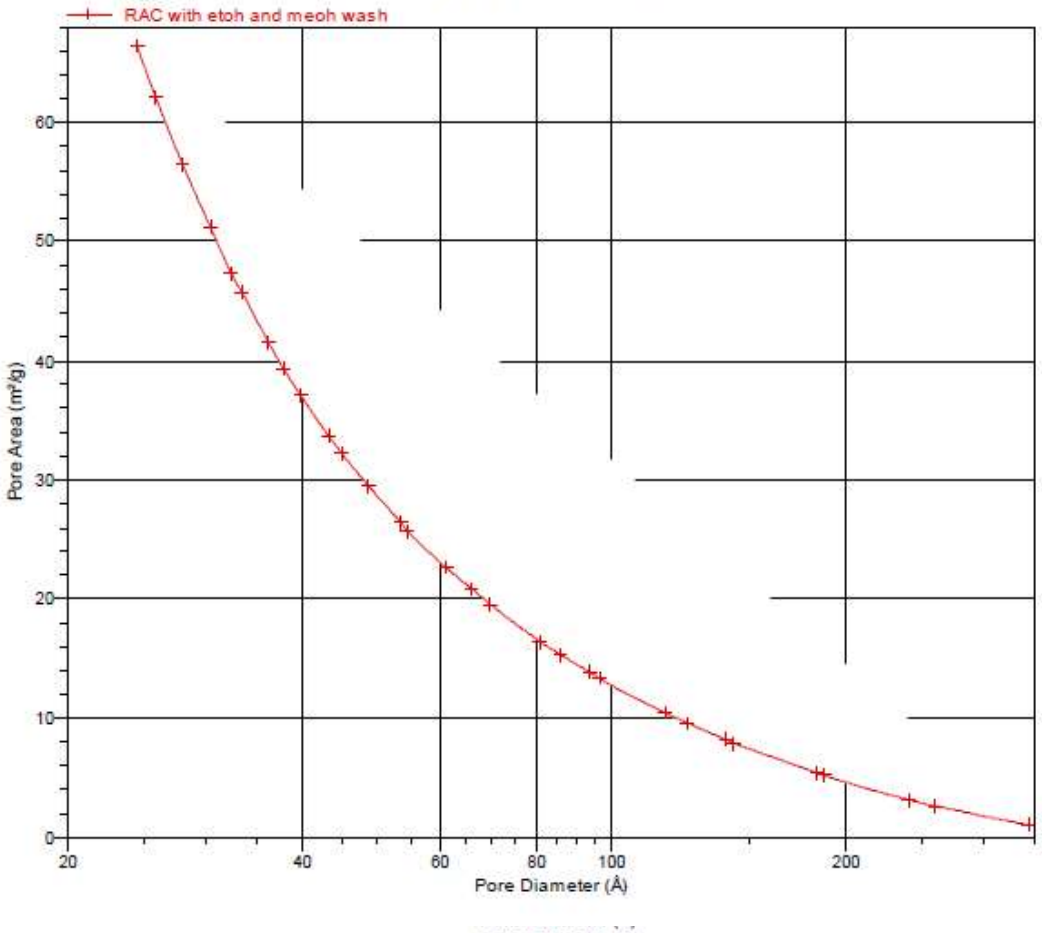

Sample: RAC with etoh and meoh wash
Operator: Akshay
Submitter:
File: C:\TriSt..\2018 10 26 RAC with etoh and meoh wash.SMP

Started:	10/26/2018 10:19:32 AM	Analysis Adsorptive:	N2
Completed:	10/26/2018 8:06:01 PM	Analysis Bath Temp.:	-195.800 °C
Report Time:	10/29/2018 2:53:48 PM	Thermal Correction:	No
Sample Mass:	0.2663 g	Warm Free Space:	9.7221 cm³ Measured
Cold Free Space:	29.2109 cm³	Equilibration Interval:	5 s
Low Pressure Dose:	None	Sample Density:	1.000 g/cm³
Automatic Degas:	No		

BJH Desorption Cumulative Pore Volume (Larger)

User-Defined : Standard

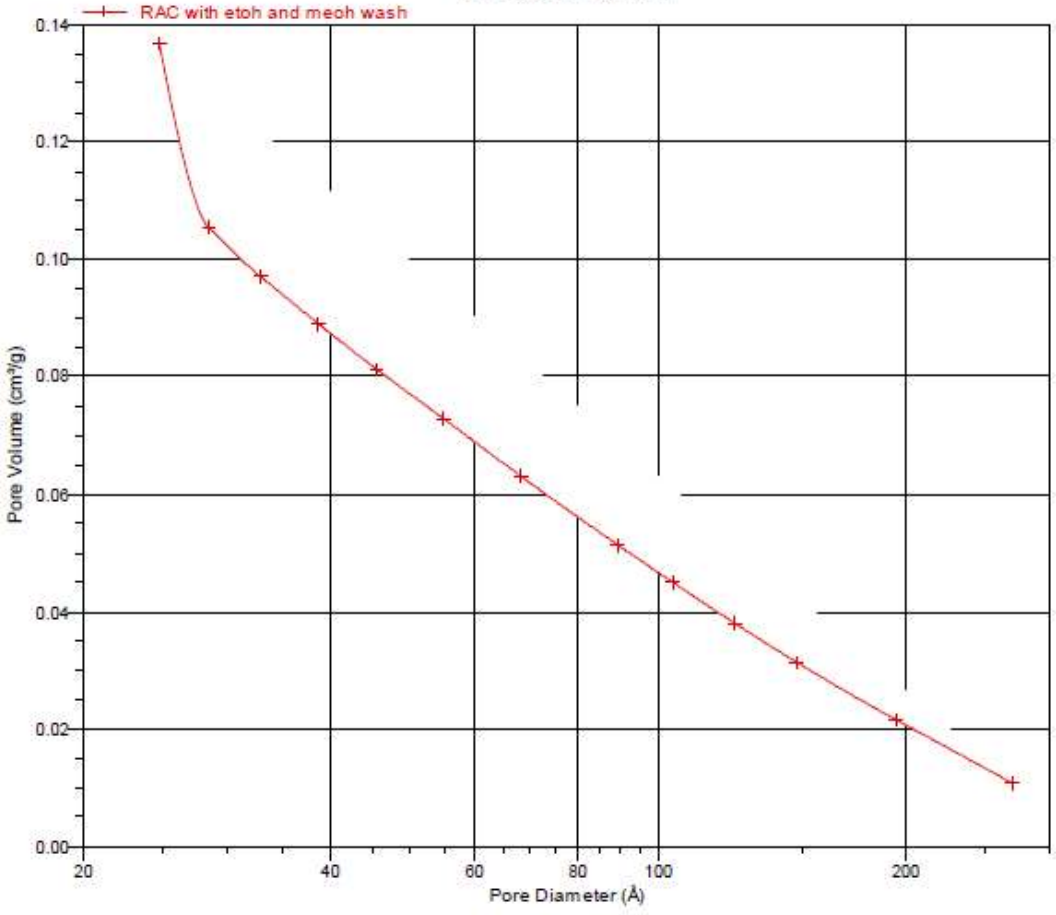

Sample: RAC with etoh and meoh wash
Operator: Akshay
Submitter:
File: C:\TriSt..\2018 10 26 RAC with etoh and meoh wash.SMP

Started:	10/26/2018 10:19:32 AM	Analysis Adsorptive:	N2
Completed:	10/26/2018 8:06:01 PM	Analysis Bath Temp.:	-195.800 °C
Report Time:	10/29/2018 2:53:48 PM	Thermal Correction:	No
Sample Mass:	0.2663 g	Warm Free Space:	9.7221 cm³ Measured
Cold Free Space:	29.2109 cm³	Equilibration Interval:	5 s
Low Pressure Dose:	None	Sample Density:	1.000 g/cm³
Automatic Degas:	No		

BJH Desorption Cumulative Pore Area (Larger)

User-Defined : Standard

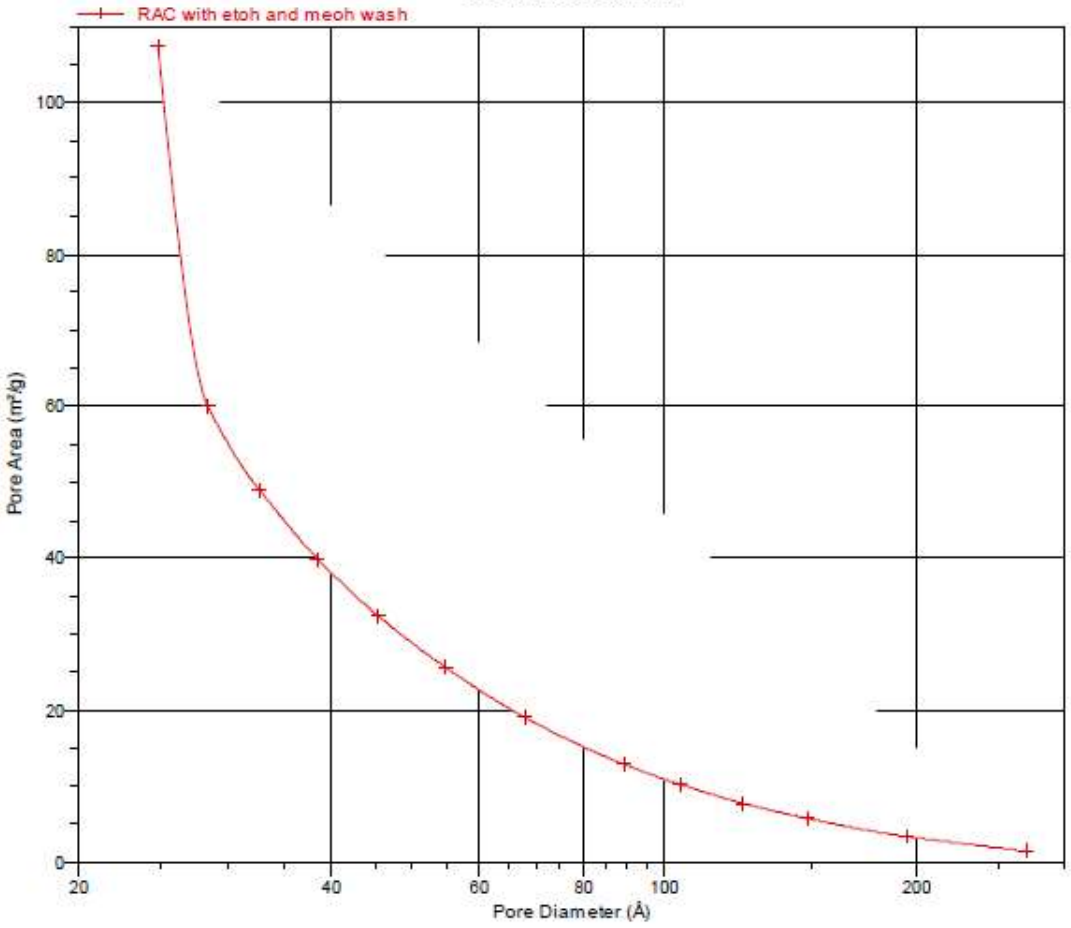

References

Aleksandrov, Krasimir, Hans Joachim Gehrmann, Manuela Hauser, Hartmut Mätzing, Daniel Pigeon, Dieter Stapf, and Manuela Wexler. 2019. “Waste Incineration of Polytetrafluoroethylene (PTFE) to Evaluate Potential Formation of per- and Poly-Fluorinated Alkyl Substances (PFAS) in Flue Gas.” *Chemosphere* 226: 898–906. https://doi.org/10.1016/j.chemosphere.2019.03.191.

Anipsitakis, George P., and Dionysios D. Dionysiou. 2004. “Radical Generation by the Interaction of Transition Metals with Common Oxidants.” *Environmental Science and Technology* 38 (13): 3705–12. https://doi.org/10.1021/es035121o.

Appleman, Timothy D., Eric R.V. Dickenson, Christopher Bellona, and Christopher P. Higgins. 2013. “Nanofiltration and Granular Activated Carbon Treatment of Perfluoroalkyl Acids.” *Journal of Hazardous Materials* 260: 740–46. https://doi.org/10.1016/j.jhazmat.2013.06.033.

Appleman, Timothy D., Christopher P. Higgins, Oscar Quiñones, Brett J. Vanderford, Chad Kolstad, Janie C. Zeigler-Holady, and Eric R.V. Dickenson. 2014. “Treatment of Poly- and Perfluoroalkyl Substances in U.S. Full-Scale Water Treatment Systems.” *Water Research* 51: 246–55. https://doi.org/10.1016/j.watres.2013.10.067.

Arvaniti, Olga S., Yuhoon Hwang, Henrik R. Andersen, Athanasios S. Stasinakis, Nikolaos S. Thomaidis, and Maria Aloupi. 2015. “Reductive Degradation of Perfluorinated Compounds in Water Using Mg-Aminoclay Coated Nanoscale Zero Valent Iron.” *Chemical Engineering Journal* 262: 133–39. https://doi.org/10.1016/j.cej.2014.09.079.

Ateia, Mohamed, Amith Maroli, Nishanth Tharayil, and Tanju Karanfil. 2019. “The Overlooked Short- and Ultrashort-Chain Poly- and Perfluorinated Substances: A

Review." *Chemosphere* 220: 866–82. https://doi.org/10.1016/j.chemosphere.2018.12.186.

Boone, J. Scott, Craig Vigo, Tripp Boone, Christian Byrne, Joseph Ferrario, Robert Benson, Joyce Donohue, et al. 2019. "Per- and Polyfluoroalkyl Substances in Source and Treated Drinking Waters of the United States." *Science of the Total Environment* 653: 359–69. https://doi.org/10.1016/j.scitotenv.2018.10.245.

Bruton, Thomas A., and David L. Sedlak. 2017. "Treatment of Aqueous Film-Forming Foam by Heat-Activated Persulfate under Conditions Representative of in Situ Chemical Oxidation." *Environmental Science and Technology* 51 (23): 13878–85. https://doi.org/10.1021/acs.est.7b03969.

Bruton, Thomas A., and David L. Sedlak. 2018. "Treatment of Perfluoroalkyl Acids by Heat-Activated Persulfate under Conditions Representative of in Situ Chemical Oxidation." *Chemosphere* 206: 457–64. https://doi.org/10.1016/j.chemosphere.2018.04.128.

Buck, Robert C., James Franklin, Urs Berger, Jason M. Conder, Ian T. Cousins, Pim De Voogt, Allan Astrup Jensen, Kurunthachalam Kannan, Scott A. Mabury, and Stefan P.J. van Leeuwen. 2011. "Perfluoroalkyl and Polyfluoroalkyl Substances in the Environment: Terminology, Classification, and Origins." *Integrated Environmental Assessment and Management* 7 (4): 513–41. https://doi.org/10.1002/ieam.258.

Butenhoff, John L, Shu-Ching Chang, Geary W Olsen, and Peter J Thomford. 2012. "Chronic Dietary Toxicity and Carcinogenicity Study with Potassium Perfluorooctanesulfonate in Sprague Dawley Rats." *Toxicology* 293 (1–3): 1–15. https://doi.org/10.1016/j.tox.2012.01.003.

Cagnetta, Giovanni, John Robertson, Jun Huang, Kunlun Zhang, and Gang Yu. 2016. "Mechanochemical Destruction of Halogenated Organic Pollutants: A Critical Review." *Journal of Hazardous Materials* 313: 85–102.

https://doi.org/10.1016/j.jhazmat.2016.03.076.

Campbell, Tammy, and Michael R. Hoffmann. 2015. “Sonochemical Degradation of Perfluorinated Surfactants: Power and Multiple Frequency Effects.” *Separation and Purification Technology* 156 (April): 1019–27. https://doi.org/10.1016/j.seppur.2015.09.053.

Carter, Kimberly E., and James Farrell. 2010. “Removal of Perfluorooctane and Perfluorobutane Sulfonate from Water via Carbon Adsorption and Ion Exchange.” *Separation Science and Technology* 45 (6): 762–67. https://doi.org/10.1080/01496391003608421.

Chen, Zhanghao, Chen Li, Juan Gao, Hailiang Dong, Yi Chen, Bing Wu, and Cheng Gu. 2020. “Efficient Reductive Destruction of Perfluoroalkyl Substances under Self-Assembled Micelle Confinement.” *Environmental Science & Technology* 54 (8): 5178–85. https://doi.org/10.1021/acs.est.9b06599.

Choi, Hyeok, Souhail R. Al-Abed, Shirish Agarwal, and Dionysios D. Dionysiou. 2008. “Synthesis of Reactive Nano-Fe/Pd Bimetallic System-Impregnated Activated Carbon for the Simultaneous Adsorption and Dechlorination of PCBs.” *Chemistry of Materials* 20 (11): 3649–55. https://doi.org/10.1021/cm8003613.

Choi, Hyeok, and Souhail R Al-Abed. 2010. “Effect of Reaction Environments on the Reactivity of PCB (2-Chlorobiphenyl) over Activated Carbon Impregnated with Palladized Iron.” *Journal of Hazardous Materials* 179 (1): 869–74. https://doi.org/10.1016/j.jhazmat.2010.03.085.

Choi, Hyeok, Souhail R Al-Abed, and Shirish Agarwal. 2009. “Effects of Aging and Oxidation of Palladized Iron Embedded in Activated Carbon on the Dechlorination of 2-Chlorobiphenyl.” *Environmental Science & Technology* 43 (11): 4137–42. http://www.ncbi.nlm.nih.gov/pubmed/19569342.

Corsini, Emanuela, Enrico Sangiovanni, Anna Avogadro, Valentina Galbiati, Barbara Viviani, Marina Marinovich, Corrado L Galli, Mario Dell'Agli, and Dori R Germolec. 2012. "In Vitro Characterization of the Immunotoxic Potential of Several Perfluorinated Compounds (PFCs)." *Toxicology and Applied Pharmacology* 258 (2): 248–55. https://doi.org/10.1016/j.taap.2011.11.004.

Flores, Cintia, Francesc Ventura, Jordi Martin-Alonso, and Josep Caixach. 2013. "Occurrence of Perfluorooctane Sulfonate (PFOS) and Perfluorooctanoate (PFOA) in N.E. Spanish Surface Waters and Their Removal in a Drinking Water Treatment Plant That Combines Conventional and Advanced Treatments in Parallel Lines." *Science of the Total Environment* 461–462: 618–26. https://doi.org/10.1016/j.scitotenv.2013.05.026.

Fu, Fenglian, Dionysios D. Dionysiou, and Hong Liu. 2014. "The Use of Zero-Valent Iron for Groundwater Remediation and Wastewater Treatment: A Review." *Journal of Hazardous Materials* 267: 194–205. https://doi.org/10.1016/j.jhazmat.2013.12.062.

Gagliano, Erica, Massimiliano Sgroi, Pietro P. Falciglia, Federico G.A. Vagliasindi, and Paolo Roccaro. 2020. "Removal of Poly- and Perfluoroalkyl Substances (PFAS) from Water by Adsorption: Role of PFAS Chain Length, Effect of Organic Matter and Challenges in Adsorbent Regeneration." *Water Research* 171: 115381. https://doi.org/10.1016/j.watres.2019.115381.

Ghabbour, Elham A., Geoffrey Davies, Nicolas P. Cuozzo, and Robert O. Miller. 2014. "Optimized Conditions for Determination of Total Soil Organic Matter in Diverse Samples by Mass Loss on Ignition." *Journal of Plant Nutrition and Soil Science* 177 (6): 914–19. https://doi.org/10.1002/jpln.201400326.

Gu, Yawei, Binbin Wang, Feng He, Miranda J. Bradley, and Paul G. Tratnyek. 2017. "Mechanochemically Sulfidated Microscale Zero Valent Iron: Pathways, Kinetics,

Mechanism, and Efficiency of Trichloroethylene Dechlorination." *Environmental Science and Technology* 51 (21): 12653–62. https://doi.org/10.1021/acs.est.7b03604.

Gu, Yurong, Tongzhou Liu, Hongjie Wang, Huili Han, and Wenyi Dong. 2017. "Hydrated Electron Based Decomposition of Perfluorooctane Sulfonate (PFOS) in the VUV/Sulfite System." *Science of the Total Environment* 607–608: 541–48. https://doi.org/10.1016/j.scitotenv.2017.06.197.

Hori, Hisao, Misako Murayama, Naoko Inoue, Kyoko Ishida, and Shuzo Kutsuna. 2010. "Efficient Mineralization of Hydroperfluorocarboxylic Acids with Persulfate in Hot Water." *Catalysis Today* 151 (1–2): 131–36. https://doi.org/10.1016/j.cattod.2010.02.023.

Hori, Hisao, Yumiko Nagaoka, Ari Yamamoto, Taizo Sano, Nobuyoshi Yamashita, Sachi Taniyasu, Shuzo Kutsuna, Ryuichi Arakawa, and Issey Osaka. 2006. "Efficient Decomposition of Environmentally Persistent Perfluorooctanesulfonate and Related Fluorochemicals Using Zerovalent Iron in Subcritical Water." *Environmental Science & Technology* 40 (3): 1049–54. https://doi.org/10.10.1021/es0517419.

Houde, Magali, Amila O De Silva, Derek C G Muir, and Robert J Letcher. 2011. "Monitoring of Perfluorinated Compounds in Aquatic Biota: An Updated Review." *Environmental Science & Technology* 45 (19): 7962. http://www.ncbi.nlm.nih.gov/pubmed/21542574.

Huang, Shan, and Peter R. Jaffé. 2019. "Defluorination of Perfluorooctanoic Acid (PFOA) and Perfluorooctane Sulfonate (PFOS) by Acidimicrobium Sp. Strain A6." *Environmental Science and Technology*. https://doi.org/10.1021/acs.est.9b04047.

Hutson, Andy, Saebom Ko, and Scott G. Huling. 2012. "Persulfate Oxidation Regeneration of Granular Activated Carbon: Reversible Impacts on Sorption Behavior."

Chemosphere 89 (10): 1218–23. https://doi.org/10.1016/j.chemosphere.2012.07.040.

Kah, Melanie, Gabriel Sigmund, Feng Xiao, and Thilo Hofmann. 2017. “Sorption of Ionizable and Ionic Organic Compounds to Biochar, Activated Carbon and Other Carbonaceous Materials.” *Water Research* 124: 673–92. https://doi.org/10.1016/j.watres.2017.07.070.

Kammerer, Judith, Reinhold Carle, and Dietmar R Kammerer. 2011. “Adsorption and Ion Exchange: Basic Principles and Their Application in Food Processing.” *Journal of Agricultural and Food Chemistry* 59 (1): 22–42. http://www.ncbi.nlm.nih.gov/pubmed/21138248.

Kannan, Kurunthachalam, Simonetta Corsolini, Jerzy Falandysz, Gilberto Fillmann, Kurunthachalam Senthil Kumar, Bommanna G Loganathan, Mustafa Ali Mohd, et al. 2004. “Perfluorooctanesulfonate and Related Fluorochemicals in Human Blood from Several Countries.” *Environmental Science & Technology* 38 (17): 4489–95. https://doi.org/10.1021/es0493446.

Kim, Cheolyong, Jun Young Ahn, Tae Yoo Kim, Won Sik Shin, and Inseong Hwang. 2018. “Activation of Persulfate by Nanosized Zero-Valent Iron (NZVI): Mechanisms and Transformation Products of NZVI.” *Environmental Science and Technology* 52 (6): 3625–33. https://doi.org/10.1021/acs.est.7b05847.

Kolthoff, I. M., and I. K. Miller. 1951. “The Chemistry of Persulfate. I. The Kinetics and Mechanism of the Decomposition of the Persulfate Ion in Aqueous Medium.” *Journal of the American Chemical Society* 73 (7): 3055–59. https://doi.org/10.1021/ja01151a024.

Kothawala, Dolly N., Stephan J. Köhler, Anna Östlund, Karin Wiberg, and Lutz Ahrens. 2017. “Influence of Dissolved Organic Matter Concentration and Composition on the

Removal Efficiency of Perfluoroalkyl Substances (PFASs) during Drinking Water Treatment." *Water Research* 121: 320–28. https://doi.org/10.1016/j.watres.2017.05.047.

Kucharzyk, Katarzyna H., Ramona Darlington, Mark Benotti, Rula Deeb, and Elisabeth Hawley. 2017. "Novel Treatment Technologies for PFAS Compounds: A Critical Review SUPP." *Journal of Environmental Management*.

Lawal, Wasiu A., and Hyeok Choi. 2018. "Feasibility Study on the Removal of Perfluorooctanoic Acid by Using Palladium-Doped Nanoscale Zerovalent Iron." *Journal of Environmental Engineering (United States)* 144 (11). https://doi.org/10.1061/(ASCE)EE.1943-7870.0001468.

Lee, Changha, Hak Hyeon Kim, and Noh Back Park. 2018. "Chemistry of Persulfates for the Oxidation of Organic Contaminants in Water." *Membrane Water Treatment* 9 (6): 405–19. https://doi.org/10.12989/mwt.2018.9.6.405.

Lee, Yu Chi, Shang Lien Lo, Pei Te Chiueh, and Der Guang Chang. 2009. "Efficient Decomposition of Perfluorocarboxylic Acids in Aqueous Solution Using Microwave-Induced Persulfate." *Water Research* 43 (11): 2811–16. https://doi.org/10.1016/j.watres.2009.03.052.

Lee, Yu Chi, Shang Lien Lo, Jeff Kuo, and Chin Pao Huang. 2013. "Promoted Degradation of Perfluorooctanic Acid by Persulfate When Adding Activated Carbon." *Journal of Hazardous Materials* 261: 463–69. https://doi.org/10.1016/j.jhazmat.2013.07.054.

Lee, Yuchi, Shanglien Lo, Jeff Kuo, and Chinghong Hsieh. 2012. "Decomposition of Perfluorooctanoic Acid by Microwaveactivated Persulfate : Effects of Temperature, PH, and Chloride Ions." *Frontiers of Environmental Science & Engineering* 6 (1): 17–25. https://doi.org/10.1007/s11783-011-0371-x.

Lei, Yong-jia, Yu Tian, Zahra Sobhani, Ravi Naidu, and Cheng Fang. 2020. "Synergistic

Degradation of PFAS in Water and Soil by Dual-Frequency Ultrasonic Activated Persulfate." *Chemical Engineering Journal* 388 (December 2019): 124215. https://doi.org/10.1016/j.cej.2020.124215.

LeVan, Douglas M, Giorgio Carta, and Carmen M You. 1999. "Adsorption and Ion Exchange." In *Perry's Chemical Engineers' Handbook*, edited by Robert H Perry and Don W Green, 9th ed., 16–66. McGraw Hill.

Li, Meng, Xiaofang Yang, DongSheng Wang, and Jin Yuan. 2017. "Enhanced Oxidation of Erythromycin by Persulfate Activated Iron Powder–H2O2 System: Role of the Surface Fe Species and Synergistic Effect of Hydroxyl and Sulfate Radicals." *Chemical Engineering Journal* 317: 103–11. https://doi.org/10.1016/j.cej.2016.12.126.

Li, Yasong, Danielle P Oliver, and Rai s. Kookana. 2018. "A Critical Analysis of Published Data to Discern the Role of Soil and Sediment Properties in Determining Sorption of per and Polyfluoroalkyl Substances (PFASs)
." *Science of the Total Environment* 628–629: 110–20. http://catalog.crl.edu/record=b1298097.

Liang, Chenju, and Hsin Wey Su. 2009. "Identification of Sulfate and Hydroxyl Radicals in Thermally Activated Persulfate." *Industrial and Engineering Chemistry Research* 48 (11): 5558–62. https://doi.org/10.1021/ie9002848.

Lindstrom, Andrew B., Mark J. Strynar, and E. Laurence Libelo. 2011. "Polyfluorinated Compounds: Past, Present, and Future." *Environmental Science and Technology* 45 (19): 7954–61. https://doi.org/10.1021/es2011622.

Liu, C. S., C. P. Higgins, F. Wang, and K. Shih. 2012. "Effect of Temperature on Oxidative Transformation of Perfluorooctanoic Acid (PFOA) by Persulfate Activation in Water." *Separation and Purification Technology* 91: 46–51. https://doi.org/10.1016/j.seppur.2011.09.047.

Liu, Jinxia, Ning Wang, Bogdan Szostek, Robert C. Buck, Patricia K. Panciroli, Patrick W. Folsom, Lisa M. Sulecki, and Cheryl A. Bellin. 2010. “6-2 Fluorotelomer Alcohol Aerobic Biodegradation in Soil and Mixed Bacterial Culture.” *Chemosphere* 78 (4): 437–44. https://doi.org/10.1016/j.chemosphere.2009.10.044.

Liu, Yueqiang, Hyeok Choi, Dionysios Dionysiou, and Gregory V Lowry. 2005. “Trichloroethene Hydrodechlorination in Water by Highly Disordered Monometallic Nanoiron.” *Chemistry of Materials* 17 (21): 5315–22. https://doi.org/10.1021/cm0511217.

McCleaf, Philip, Sophie Englund, Anna Östlund, Klara Lindegren, Karin Wiberg, and Lutz Ahrens. 2017. “Removal Efficiency of Multiple Poly- and Perfluoroalkyl Substances (PFASs) in Drinking Water Using Granular Activated Carbon (GAC) and Anion Exchange (AE) Column Tests.” *Water Research* 120: 77–87. https://doi.org/10.1016/j.watres.2017.04.057.

Merino, Nancy, Yan Qu, Rula A. Deeb, Elisabeth L. Hawley, Michael R. Hoffmann, and Shaily Mahendra. 2016. “Degradation and Removal Methods for Perfluoroalkyl and Polyfluoroalkyl Substances in Water.” *Environmental Engineering Science* 33 (9): 615–49. https://doi.org/10.1089/ees.2016.0233.

Milinovic, Jelena, Silvia Lacorte, Miquel Vidal, and Anna Rigol. 2015. “Sorption Behaviour of Perfluoroalkyl Substances in Soils.” *Science of the Total Environment* 511: 63–71. https://doi.org/10.1016/j.scitotenv.2014.12.017.

Nfodzo, Prince, Choi, Hyeok (2011)."Triclosan decomposition by sulfate radicals: effects of oxidant and metal doses." Chemical Engineering Journal 174, 629-634.

Ochiai, Tsuyoshi, Yuichi Iizuka, Kazuya Nakata, Taketoshi Murakami, Donald A. Tryk, Akira Fujishima, Yoshihiro Koide, and Yuko Morito. 2011. “Efficient Electrochemical Decomposition of Perfluorocarboxylic Acids by the Use of a Boron-Doped Diamond

Electrode." *Diamond and Related Materials* 20 (2): 64–67. https://doi.org/10.1016/j.diamond.2010.12.008.

Ochoa-Herrera, Valeria, and Reyes Sierra-Alvarez. 2008. "Removal of Perfluorinated Surfactants by Sorption onto Granular Activated Carbon, Zeolite and Sludge." *Chemosphere* 72 (10): 1588–93. https://doi.org/10.1016/j.chemosphere.2008.04.029.

Organisation for Economic Cooperation and Development (OECD/UNEP) Global PFC Group. 2013. "United Nations Environment Programme: Synthesis Paper on per- and Polyfluorinated Chemicals (PFCs), Environment, Health and Safety, Environment Directorate, OECD." *IOMC: Inter-Organization Programme for the Sound Managment of Chemicals*, 1–58.

Organisation for Economic Cooperation and Development (OECD). 2015. "OECD Environment, Health and Safety Publications Series on Risk Management No. 30: Working Towards a Global Emission Inventory of PFASs: Focus on PFCAs - Status Quo and the Way Forward." *Health and Safety Publications Series on Risk Management* 30: 33. http://www.oecd.org/chemicalsafety/risk-management/Working Towards a Global Emission Inventory of PFASS.pdf.

Parenky, A. C., Gevaerd de Souza, N., Asgari, P., Jeon, J., Nadagouda, M. N., Choi, H. 2020. "Removal of Perfluorooctanesulfonic Acid (PFOS) in Water by Combining Zerovalent Iron Particles with Common Oxidants." *Environmental Engineering Science.* 37 (7): 472-481. http://doi.org/10.1089/ees.2019.0406

Park, Hyunwoong, Chad D. Vecitis, Jie Cheng, Wonyong Choi, Brian T. Mader, and Michael R. Hoffmann. 2009. "Reductive Defluorination of Aqueous Perfluorinated Alkyl Surfactants: Effects of Ionic Headgroup and Chain Length." *Journal of Physical Chemistry A* 113 (4): 690–96. https://doi.org/10.1021/jp807116q.

Park, Minkyu, Shimin Wu, Israel J. Lopez, Joseph Y. Chang, Tanju Karanfil, and Shane A. Snyder. 2020. “Adsorption of Perfluoroalkyl Substances (PFAS) in Groundwater by Granular Activated Carbons: Roles of Hydrophobicity of PFAS and Carbon Characteristics.” *Water Research* 170 (March): 115364. https://doi.org/10.1016/j.watres.2019.115364.

Park, Saerom, Linda S. Lee, Victor F. Medina, Aaron Zull, and Scott Waisner. 2016. “Heat-Activated Persulfate Oxidation of PFOA, 6:2 Fluorotelomer Sulfonate, and PFOS under Conditions Suitable for in-Situ Groundwater Remediation.” *Chemosphere* 145: 376–83. https://doi.org/10.1016/j.chemosphere.2015.11.097.

Park, Saerom, Jenny E. Zenobio, and Linda S. Lee. 2018. “Perfluorooctane Sulfonate (PFOS) Removal with Pd0/NFe0 Nanoparticles: Adsorption or Aqueous Fe-Complexation, Not Transformation?” *Journal of Hazardous Materials* 342: 20–28. https://doi.org/10.1016/j.jhazmat.2017.08.001.

Paul, Alexander G., Kevin C. Jones, and Andrew J. Sweetman. 2009. “A First Global Production, Emission, and Environmental Inventory for Perfluorooctane Sulfonate.” *Environmental Science and Technology* 43 (2): 386–92. https://doi.org/10.1021/es802216n.

Rahman, Mohammad Feisal, Sigrid Peldszus, and William B Anderson. 2014. “Behaviour and Fate of Perfluoroalkyl and Polyfluoroalkyl Substances (PFASs) in Drinking Water Treatment: A Review.” *Water Research* 50: 318. https://doi.org/10.1016/j.watres.2013.10.045.

Rayne, Sierra, and Kaya Forest. 2009. “Perfluoroalkyl Sulfonic and Carboxylic Acids: A Critical Review of Physicochemical Properties, Levels and Patterns in Waters and Wastewaters, and Treatment Methods.” *Journal of Environmental Science and Health - Part A Toxic/Hazardous Substances and Environmental Engineering* 44 (12):

1145–99. https://doi.org/10.1080/10934520903139811.

Ross, Ian, Jeffrey McDonough, Jonathan Miles, Peter Storch, Parvathy Thelakkat Kochunarayanan, Erica Kalve, Jake Hurst, Soumitri S. Dasgupta, and Jeff Burdick. 2018. “A Review of Emerging Technologies for Remediation of PFASs.” *Remediation* 28 (2): 101–26. https://doi.org/10.1002/rem.21553.

Sedlak, Margaret D, Jonathan P Benskin, Adam Wong, Richard Grace, and Denise J Greig. 2017. “Per-and Polyfluoroalkyl Substances (PFASs) in San Francisco Bay Wildlife: Temporal Trends, Exposure Pathways, and Notable Presence of Precursor Compounds.” *Chemosphere* 185: 1217. http://urn.kb.se/resolve?urn=urn:nbn:se:su:diva-146948.

Silva-Rackov, Celyna K O da, Wasiu A Lawal, Prince A Nfodzo, Marilda M G R Vianna, Claudio A O do Nascimento, and Hyeok Choi. 2016. “Degradation of PFOA by Hydrogen Peroxide and Persulfate Activated by Iron-Modified Diatomite.” *Applied Catalysis B: Environmental* 192: 253–59. https://doi.org/10.1016/j.apcatb.2016.03.067.

Solo-Gabriele, Helena M., Athena S. Jones, Andrew B. Lindstrom, and Johnsie R. Lang. 2020. “Waste Type, Incineration, and Aeration Are Associated with per- and Polyfluoroalkyl Levels in Landfill Leachates.” *Waste Management* 107 (May 2016): 191–200. https://doi.org/10.1016/j.wasman.2020.03.034.

Sorengard, M., Dan Berggren Kleja, and Lutz Ahrens. 2019. “Stabilization of Per- and Polyfluoroalkyl Substances (PFASs) with Colloidal Activated Carbon (PlumeStop®) as a Function of Soil Clay and Organic Matter Content.” *Journal of Environmental Management* 249 (July): 109345. https://doi.org/10.1016/j.jenvman.2019.109345.

Tang, Chuyang Y., Q. Shiang Fu, Craig S. Criddle, and James O. Leckie. 2007. “Effect of Flux (Transmembrane Pressure) and Membrane Properties on Fouling and Rejection

of Reverse Osmosis and Nanofiltration Membranes Treating Perfluorooctane Sulfonate Containing Wastewater." *Environmental Science and Technology* 41 (6): 2008–14. https://doi.org/10.1021/es062052f.

Tang, Heqing, Qingqing Xiang, Min Lei, Jingchun Yan, Lihua Zhu, and Jing Zou. 2012. "Efficient Degradation of Perfluorooctanoic Acid by UV–Fenton Process." *Chemical Engineering Journal* 184: 156–62. https://doi.org/10.1016/j.cej.2012.01.020.

Tanner, Eva, Michael Bloom, Qian Wu, Kurunthachalam Kannan, Recai Yucel, Srishti Shrestha, and Edward Fitzgerald. 2018. "Occupational Exposure to Perfluoroalkyl Substances and Serum Levels of Perfluorooctanesulfonic Acid (PFOS) and Perfluorooctanoic Acid (PFOA) in an Aging Population from Upstate New York: A Retrospective Cohort Study." *International Archives of Occupational and Environmental Health* 91 (2): 145–54. https://doi.org/10.1007/s00420-017-1267-2.

Thompson, Jack, Geoff Eaglesham, Julien Reungoat, Yvan Poussade, Michael Bartkow, Michael Lawrence, and Jochen F. Mueller. 2011. "Removal of PFOS, PFOA and Other Perfluoroalkyl Acids at Water Reclamation Plants in South East Queensland Australia." *Chemosphere* 82 (1): 9–17. https://doi.org/10.1016/j.chemosphere.2010.10.040.

Trojanowicz, Marek, Anna Bojanowska-Czajka, Iwona Bartosiewicz, and Krzysztof Kulisa. 2018. "Advanced Oxidation/Reduction Processes Treatment for Aqueous Perfluorooctanoate (PFOA) and Perfluorooctanesulfonate (PFOS) – A Review of Recent Advances." *Chemical Engineering Journal* 336 (August 2017): 170–99. https://doi.org/10.1016/j.cej.2017.10.153.

United Nations Environment Programme (UNEP). 2014 Stockholm Convention on Persistent Organic Pollutants. http://www.pops.int/Implementation/IndustrialPOPs/Overview/tabid/5221/Default.aspx

US Environmental Protection Agency (USEPA), National Priorities: PER- AND POLYFLUOROALKYL SUBSTANCES (EPA-G2018-ORD-A1). 2018 Retrieved from https://www.epa.gov/research-grants/national-priorities-and-polyfluoroalkyl-substances

US Environmental Protection Agency (USEPA), Drinking Water Health Advisories for PFOA and PFOS (EPA-HQ-OW-2014-0138; FRL-9946-91-OW). 2016 Retrieved from https://www.epa.gov/ground-water-and-drinking-water/drinking-water-health-advisories-pfoa-and-pfos.pdf

US Environmental Protection Agency (USEPA), Third Unregulated Contaminant Monitoring Rule (EPA 815-F-16-003) 2012. Fed. Regist. 76 (42), 11713-11737

Vecitis, Chad D., Hyunwoong Park, Jie Cheng, Brian T. Mader, and Michael R. Hoffmann. 2009. “Treatment Technologies for Aqueous Perfluorooctanesulfonate (PFOS) and Perfluorooctanoate (PFOA).” *Frontiers of Environmental Science and Engineering in China* 3 (2): 129–51. https://doi.org/10.1007/s11783-009-0022-7.

Wacławek, Stanisław, Holger V. Lutze, Klaudiusz Grübel, Vinod V.T. Padil, Miroslav Černík, and Dionysios D. Dionysiou. 2017. “Chemistry of Persulfates in Water and Wastewater Treatment: A Review.” *Chemical Engineering Journal* 330 (July): 44–62. https://doi.org/10.1016/j.cej.2017.07.132.

Wang, Fei, Xingwen Lu, Xiao Yan Li, and Kaimin Shih. 2015. “Effectiveness and Mechanisms of Defluorination of Perfluorinated Alkyl Substances by Calcium Compounds during Waste Thermal Treatment.” *Environmental Science and Technology* 49 (9): 5672–80. https://doi.org/10.1021/es506234b.

Wang, Fei, and Kaimin Shih. 2011. “Adsorption of Perfluorooctanesulfonate (PFOS) and Perfluorooctanoate (PFOA) on Alumina: Influence of Solution PH and Cations.” *Water Research* 45 (9): 2925–30. https://doi.org/10.1016/j.watres.2011.03.007.

Wang, Fei, Kaimin Shih, Ruowei Ma, and Xiao-yan Li. 2015. “Influence of Cations on the Partition Behavior of Perfluoroheptanoate (PFHpA) and Perfluorohexanesulfonate (PFHxS) on Wastewater Sludge.” *Chemosphere* 131: 178–83. https://doi.org/10.1016/j.chemosphere.2015.03.024.

Wang, Jianlong, and Shizong Wang. 2018. “Activation of Persulfate (PS) and Peroxymonosulfate (PMS) and Application for the Degradation Emerging Contaminants.” *Chemical Engineering Journal* 334: 1502–17. https://doi.org/10.1016/j.cej.2016.10.064.

Wang, Li, Bill Batchelor, Suresh D. Pillai, and Venkata S.V. Botlaguduru. 2016. “Electron Beam Treatment for Potable Water Reuse: Removal of Bromate and Perfluorooctanoic Acid.” *Chemical Engineering Journal* 302 (October): 58–68. https://doi.org/10.1016/j.cej.2016.05.034.

Wang, Lu, Junhe Lu, Lei Li, Yaye Wang, and Qingguo Huang. 2020. “Effects of Chloride on Electrochemical Degradation of Perfluorooctanesulfonate by Magnéli Phase Ti4O7 and Boron Doped Diamond Anodes.” *Water Research* 170: 115254. https://doi.org/10.1016/j.watres.2019.115254.

Wang, Zhanyun, Jamie C. Dewitt, Christopher P. Higgins, and Ian T. Cousins. 2017. “A Never-Ending Story of Per- and Polyfluoroalkyl Substances (PFASs)?” *Environmental Science and Technology* 51 (5): 2508–18. https://doi.org/10.1021/acs.est.6b04806.

Wu, Boran, Shilai Hao, Younjeong Choi, Christopher P. Higgins, Rula Deeb, and Timothy J. Strathmann. 2019. “Rapid Destruction and Defluorination of Perfluorooctanesulfonate by Alkaline Hydrothermal Reaction.” *Environmental Science and Technology Letters* 6 (10): 630–36. https://doi.org/10.1021/acs.estlett.9b00506.

Xiao, Feng. 2017. “Emerging Poly- and Perfluoroalkyl Substances in the Aquatic Environment: A Review of Current Literature.” *Water Research* 124: 482–95. https://doi.org/10.1016/j.watres.2017.07.024.

Xiao, Feng, Kerry Jade Davidsavor, Sangyoo Park, Michio Nakayama, and Brian Ray Phillips. 2012. “Batch and Column Study: Sorption of Perfluorinated Surfactants from Water and Cosolvent Systems by Amberlite XAD Resins.” *Journal of Colloid and Interface Science* 368 (1): 505–11. https://doi.org/10.1016/j.jcis.2011.11.011.

Xiao, Leilei, Yuhan Ling, Alaaeddin Alsbaiee, Chenjun Li, Damian E. Helbling, and William R. Dichtel. 2017. “β-Cyclodextrin Polymer Network Sequesters Perfluorooctanoic Acid at Environmentally Relevant Concentrations.” *Journal of the American Chemical Society* 139 (23): 7689–92. https://doi.org/10.1021/jacs.7b02381.

Xiao, Xin, Bridget A. Ulrich, Baoliang Chen, and Christopher P. Higgins. 2017. “Sorption of Poly- and Perfluoroalkyl Substances (PFASs) Relevant to Aqueous Film-Forming Foam (AFFF)-Impacted Groundwater by Biochars and Activated Carbon.” *Environmental Science and Technology* 51 (11): 6342–51. https://doi.org/10.1021/acs.est.7b00970.

Xie, Yingying, Zhanqiang Fang, Xinhong Qiu, Eric Pokeung Tsang, and Bin Liang. 2014. “Comparisons of the Reactivity, Reusability and Stability of Four Different Zero-Valent Iron-Based Nanoparticles.” *Chemosphere* 108: 433–36. https://doi.org/10.1016/j.chemosphere.2014.01.076.

Yu, Qiang, Ruiqi Zhang, Shubo Deng, Jun Huang, and Gang Yu. 2009. “Sorption of Perfluorooctane Sulfonate and Perfluorooctanoate on Activated Carbons and Resin: Kinetic and Isotherm Study.” *Water Research* 43 (4): 1150–58. https://doi.org/10.1016/j.watres.2008.12.001.

Zenobio, Jenny E., Mahsa Modiri-Gharehveran, Chloe de Perre, Chad D. Vecitis, and

Linda S. Lee. 2020. “Reductive Transformation of Perfluorooctanesulfonate by NNiFe0-Activated Carbon.” *Journal of Hazardous Materials* 397 (November 2019): 122782. https://doi.org/10.1016/j.jhazmat.2020.122782.

Zhang, D. Q., W. L. Zhang, and Y. N. Liang. 2019. “Adsorption of Perfluoroalkyl and Polyfluoroalkyl Substances (PFASs) from Aqueous Solution - A Review.” *Science of the Total Environment* 694. https://doi.org/10.1016/j.scitotenv.2019.133606.

Zhang, Yanyan, Jinxia Liu, Audrey Moores, and Subhasis Ghoshal. 2020. “Transformation of 6:2 Fluorotelomer Sulfonate by Cobalt(II)-Activated Peroxymonosulfate.” *Environmental Science and Technology* 54 (7): 4631–40. https://doi.org/10.1021/acs.est.9b07113.

Zhang, Yanyan, Audrey Moores, Jinxia Liu, and Subhasis Ghoshal. 2019. “New Insights into the Degradation Mechanism of Perfluorooctanoic Acid by Persulfate from Density Functional Theory and Experimental Data.” *Environmental Science and Technology* 53 (15): 8672–81. https://doi.org/10.1021/acs.est.9b00797.

Zhao, Lixia, Jingna Bian, Yahui Zhang, Lingyan Zhu, and Zhengtao Liu. 2014. “Comparison of the Sorption Behaviors and Mechanisms of Perfluorosulfonates and Perfluorocarboxylic Acids on Three Kinds of Clay Minerals.” *Chemosphere* 114 (May 2009): 51–58. https://doi.org/10.1016/j.chemosphere.2014.03.098.

Zhao, Lixia, Yifeng Zhang, Shuhong Fang, Lingyan Zhu, and Zhengtao Liu. 2014. “Comparative Sorption and Desorption Behaviors of PFHxS and PFOS on Sequentially Extracted Humic Substances.” *Journal of Environmental Sciences (China)* 26 (12): 2517–25. https://doi.org/10.1016/j.jes.2014.04.009.

Biographical Information

Naomi Gevaerd de Souza started her academic path in Brazil where she earned her B.S. in Biological Sciences at the Federal University of Santa Catarina while conducting research related to marine animals. Her interests eventually led her to work offshore in the oil prospection industry as a Marine Mammal Observer, Passive Acoustic Monitoring operator, and Environmental Technician in several countries. Naomi also had the opportunity to teach Biology and Sciences in Middle and High Schools in Brazil, and to participate in programs to continue education for school-deprived students such as hospitalized children, expelled students, and adults that did not conclude their basics.

While conducting her graduate studies at the University of Texas at Arlington (UTA), Naomi worked with advanced oxidation applied to water remediation under the supervision of Dr. Hyeok Choi. During this period, she could also devote her time to support graduate and undergraduate Civil Engineering classes as Teaching Assistant at UTA. Naomi is very enthusiastic about Science, and she hopes to continue to dedicate her efforts to environmentally relevant issues.